Environmental Science Advances

ROYAL SOCIETY OF CHEMISTRY

PAPER

View Article Online
View Journal | View Issue

Cite this: *Environ. Sci.: Adv.*, 2025, **4**, 787

Multifunctional copolymers for brilliant green dye removal: adsorption kinetics, isotherm and process optimization†

Yassin A. Aggour,[a] El-Refaie Kenawy,[b] Marwa Magdy[a] and Elsayed Elbayoumy *[a]

The presence of toxic dyes in water stream poses a significant environmental threat to human health and aquatic life. In this study, poly(AN-*co*-AMPS) was synthesized *via* free radical copolymerization and evaluated as an adsorbent for the removal of brilliant green (BG) dye from aqueous solutions. Comprehensive characterization using FTIR spectroscopy, XRD, TGA, FESEM, EDX, XPS and BET confirmed the successful synthesis of poly(AN-*co*-AMPS) with a high surface area of 64.07 $m^2\ g^{-1}$. Adsorption studies revealed optimal removal conditions at pH 7, 298 K, 0.1 g adsorbent dosage, 7.5 mg L^{-1} initial dye concentration, and 80 min contact time, achieving a maximum removal efficiency of 99.5%. Adsorption isotherm analysis demonstrated a strong fit to the Langmuir model with a maximum adsorption capacity of 16.28 mg g^{-1}, while kinetic studies indicated a pseudo-second-order mechanism. Thermodynamic analysis confirmed that the adsorption process is spontaneous ($\Delta G < 0$) and endothermic ($\Delta H > 0$). The primary adsorption mechanisms were identified as electrostatic, hydrogen bond and $\pi-\pi$ interactions. Furthermore, regeneration studies showed that poly(AN-*co*-AMPS) maintained high stability and removal efficiency over six successive cycles. The Box–Behnken design (BBD) optimization provided a statistical model for predicting the adsorption performance under varying conditions. These findings highlight the potential of poly(AN-*co*-AMPS) as a promising, reusable adsorbent for BG dye removal from wastewater.

Received 2nd December 2024
Accepted 14th March 2025

DOI: 10.1039/d4va00404c

rsc.li/esadvances

Environmental significance

The discharge of toxic dyes such as brilliant green from industrial effluents poses significant environmental risks, including water pollution, ecosystem disruption, and threats to human health. Addressing this challenge is essential for preserving water quality and protecting biodiversity. This study introduces poly(AN-*co*-AMPS), a copolymer synthesized *via* free radical copolymerization, as an efficient and sustainable adsorbent for dye removal from wastewater. The material demonstrated high adsorption efficiency, exhibited regenerability using HCl, and maintained the performance over multiple cycles. Its application can significantly reduce dye concentrations in industrial effluents, improving water quality, safeguarding aquatic ecosystems, and minimizing health hazards for communities relying on these water sources. This approach contributes to sustainable wastewater treatment practices and promotes long-term environmental health.

1 Introduction

The rapid growth of industries and human technological advancements are leading to water pollution, which is becoming a serious environmental concern.[1–4] Organic dyes are associated with many industries including textile, paper, plastic, cosmetics, food, rubber, fiber, pesticide coloring, printing, leather, petroleum, glass, ceramics and hair dye.[5–7] They are harmful to aquatic life, and humans may have health issues such as nervous system damage, kidney diseases, skin problems like allergy, skin irritation and sensitization, genetic mutation, shortness of breath, cancer, diarrhea and abdominal pain.[8–10] Furthermore, color dyes in water will reduce light penetration, which would impede aquatic plant photosynthesis and increase the chemical oxygen demand, all of which have the potential to seriously harm the ecosystem.[11,12] Additionally, dyes can hinder the ability of gases to dissolve in water, which reduces the capacity for re-oxygenation and results in the formation of an anaerobic environment.[13] One of these harmful dyes is BG dye, a synthetic cationic dye that is hazardous and currently being utilized for various purposes, including in coloring paper, silk, wool, rubber, leather, veterinary medicine, and intestinal parasite treatment.[14,15] Aquatic life and human

[a]*Chemistry Department, Faculty of Science, Damietta University, New Damietta 34517, Egypt. E-mail: sayedelbayoumy@du.edu.eg; marwasleem@du.edu.eg; yassinag@du.edu.eg*

[b]*Polymer Research Group, Chemistry Department, Faculty of Science, Tanta University, Tanta 31527, Egypt. E-mail: ekenawy@yahoo.com*

† Electronic supplementary information (ESI) available. See DOI: https://doi.org/10.1039/d4va00404c

beings are harmed by the direct discharge of untreated BG dye into water bodies. Consequently, it is important to eliminate dye contaminants from effluents prior to their ultimate release into the environment. Various methods including membrane separation, flocculation precipitation, advanced oxidation, microbial degradation, photocatalytic degradation, electrocoagulation, adsorption and electrochemical processes have been used to extract dyes from wastewater.[16–19] Among these techniques, adsorption on the solid surface is commonly utilized due to its benefits which include high efficiency, low cost, large-scale application and easy operation.[20,21] The most important factor in adsorption technique is choosing an adsorbent with a large adsorption capacity, high efficiency, ease of manufacture, low cost and notable durability and recyclability. Some types of adsorbents such as activated carbon, graphene-based sorbents, biochar (BC), metal organic frameworks, zeolites, biomaterials, nanoparticles, porous materials, clay minerals and polymers have been used in the field of removal of dyes from wastewater.[22,23] For instance, coquina derived from oyster shells was used as a bioadsorbent to remove the BG dye from wastewater.[24] *Ficus benghalensis* tree leaves were used as adsorbents for removing the toxic BG dye from water.[25] In addition, amine-modified tannin gel (ATG) has been found to be a highly effective adsorbent for the removal of BG dye.[26] Moreover, a molecularly imprinted polymer (MIP) is also used as a selective adsorbent for BG dye removal from river and textile industry effluents.[27] Moreover, magnetic barium phosphate composites were studied as an example for the removal of an organic dye pollutant (BG) from the synthetic medium.[28] In general, polymeric materials are regarded as excellent adsorbents for removing organic and inorganic pollutants from wastewater.[29–32] Among these polymers, poly(AN-*co*-AMPS) is a vinyl copolymer that has unique structural properties. This copolymer, composed of acrylonitrile (AN) and 2-acrylamido-2-methylpropanesulfonic acid (AMPS), features a high surface area and pore volume, which enhances its capacity to absorb contaminants.[33] Moreover, it has gained to be an excellent adsorbent due to its simple fabrication, low cost, recyclability, non-hazardous, excellent sorption effectiveness, steadiness in environment and large-scale applications. The presence of multifunctional groups such as amide and sulfonic in the AMPS component in addition to the cyano group in AN is particularly advantageous, as these groups facilitate effective coordination with dye molecules. This interaction improves the efficiency of dye removal or separation, making poly(AN-*co*-AMPS) an effective material for applications in water purification and other processes where dye adsorption is crucial. Moreover, poly(AN-*co*-AMPS) has high stability that enables its large-scale applications under different operational conditions.[34–36]

In the present work, we prepared poly(AN-*co*-AMPS) *via* free radical polymerization techniques and used it as an adsorbent for the removal of BG dye from aqueous solutions (Fig. 1). The prepared copolymer was characterized by FTIR spectroscopy, SEM, XRD, TGA, EDX and BET technique. The synthesized poly(AN-*co*-AMPS) copolymer will demonstrate exceptional adsorption efficiency and reusability, making it a promising candidate for dye removal applications. Its high surface area, functional group diversity, and porous structure enhance the adsorption of Brilliant Green (BG) dye through electrostatic interactions, hydrogen bond formation and π–π interactions. The effects of contact time, adsorbent dosage, initial concentration, temperature and pH on the efficiency of dye adsorption were studied. In addition, the kinetic, isotherms and thermodynamics for the adsorption process were also evaluated to obtain information for treating wastewater containing dyes. A regeneration study was also carried out to determine whether

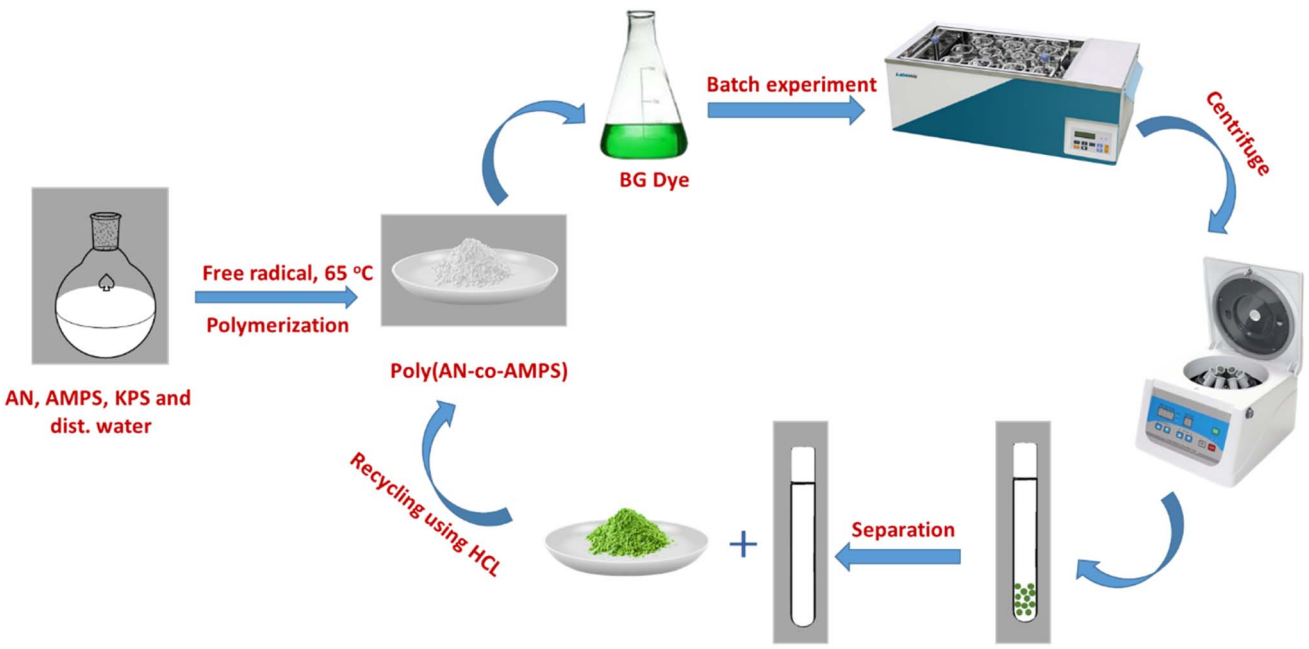

Fig. 1 Experimental design of the removal of hazardous BG dye using poly(AC-*co*-AMPS).

the prepared adsorbent could be reused. Furthermore, the Box–Behnken (BBD) design approach was used to perform RSM modeling of BG dye adsorption on poly(AN-*co*-AMPS). Finally, this work presents a viable way for using poly(AN-*co*-AMPS) to effectively remove BG dye from wastewater.

2 Materials and methods

2.1. Materials

All chemicals were used just as supplied without any further purification. 2-Acrylamido-2-methylpropane sulfonic acid (AMPS, purity > 98%) monomer was received from Fluka Company. Acrylonitrile (AN, purity 99%) monomer was purchased from Rasayan Laboratories Company. Potassium persulfate (KPS, purity > 98%) initiator was obtained from LOBA Chemie. Brilliant green dye (BG, λ_{max} = 625 nm) with the molecular formula $C_{27}H_{34}N_2O_4S$ was purchased from Aldrich chemicals. Hydrochloric acid (HCL), sodium hydroxide (NaOH) and potassium nitrate (KNO_3) with 98% purity were purchased from commercial sources. Distilled water was used as a solvent throughout the experiment.

2.2. Synthesis of poly(AN-*co*-AMPS)

In order to synthesize a poly(AN-*co*-AMPS) copolymer, a free radical copolymerization process was performed using both AN and AMPS as vinyl monomers and KPS acts as an initiator.[36,37] Briefly, AN (5.072 g, 95.7 mmol), AMPS (0.89 g, 4.3 mmol), and KPS (0.056 g, 0.21 mmol) were introduced to a 100 mL round-bottom flask attached with a condenser containing distilled water (60 mL) as the solvent. The reaction mixture was stirred until the formation of a homogeneous solution. After that the temperature of the reaction mixture was increased to 65 °C for four hours with continuous stirring. The obtained white precipitate of the copolymer was collected by filtration followed by washing with distilled water to get rid of any remaining initiator or unreacted monomers. Ultimately, the copolymer was dried overnight until its weight stabilized and yield, which was 4.08 g (68.4. %) of poly(AN-*co*-AMPS) as a white solid powder and kept in a desiccator before being used in batch BG adsorption studies.

2.3. Characterization techniques

Fourier transform infrared (FTIR) spectra was recorded using a JASCO FT/IR-6100 spectrometer with a KBr pellet sample in the scanning range of 4000–400 cm^{-1} to investigate the specific functional groups present in the copolymer. Thermogravimetric analysis (TGA) was performed using a Rigaku Thermo plus TG8120 instrument in a nitrogen gas atmosphere at a flow rate of 20 mL min^{-1} and a heating rate of 10 K min^{-1} using alumina ceramic sample pans from ambient temperature to 800 °C in order to investigate the thermal stability of the copolymer. The pore volume and surface area of the copolymer were measured by nitrogen adsorption/desorption techniques using a Quantachrome instrument (USA) based on the Brunauer–Emmett–Teller (BET) equation. Wide-angle X-ray diffraction (XRD) patterns were acquired using a Siemens D-500 X-ray diffractometer (λ = 1.54 Å (Cu Kα)) to explore the crystalline structure and crystalline size of the copolymer. Field emission scanning electron microscopic (FESEM) images were acquired using a JEM-2100F microscope at an accelerating voltage of 200 kV to investigate the micromorphological and microtextural features of the copolymer. An energy-dispersive X-ray spectrometer (EDX-map) equipped with a SUPER-X silicon-drift windowless EDX detector and an HAADF detector at 5 kV operating voltage was used to determine the elemental distribution in the samples. X-ray photoelectron spectroscopy (XPS) was recorded using an Omicron XPS spectrometer with a Mg Kα X-ray source (1254 eV) to investigate the chemical composition and bending energy of poly(AN-*co*-AMPS).

2.4. Batch adsorption experiments

The batch adsorption experiments were carried out in bottles of 150 mL capacity provided with caps at room temperature to investigate different adsorption parameters, adsorption kinetics, isotherm and thermodynamics. First, 100 mL of BG solution containing a fixed amount of adsorbent under investigation was adjusted to the required pH with specific concentration. After the addition of a known amount of adsorbent, the bottles were shaken for 120 min in a thermostatic shaker at 250 rpm. At the end of the equilibrium period, the BG solution was centrifuged and the change in dye concentration was observed using a UV-vis spectrophotometer at λ of 625 nm, which was identified as the equilibrium concentration of BG (C_e). All experiments were repeated three times for more accuracy. The effects of different adsorption parameters such as contact time (0–120 min), adsorbent dose (20–180 mg), initial dye concentration (2.5–15 mg L^{-1}), pH^{3-9} and temperature (303–331 K) were investigated during this study.

The adsorption capacity of BG adsorbed on poly(AN-*co*-AMPS) (q_t, mg g^{-1}) at time t and the percentage of dye removal (%R) were calculated based on eqn (1) and (2), respectively:

$$q_t = \frac{C_0 - C_t}{W} \times V \quad (1)$$

$$\%R = \frac{C_0 - C_t}{C_0} \times 100 \quad (2)$$

where C_0 and C_t are the concentrations of BG dye (mg L^{-1}) initially and at time t, respectively. V is the volume of BG dye solution (L) and W is the amount of the adsorbent used (g).

2.5. Regeneration experiments

The regeneration of the adsorbent reduced material cost, which is considered an important economic aspect. Through adsorption/desorption tests, the regeneration efficiency of poly(AN-*co*-AMPS) was investigated. First, the adsorption process was performed using 100 mL of BG dye solution (7.5 mg L^{-1}) and 100 mg of poly(AN-*co*-AMPS) for 60 minutes. Next, the polymer/BG dye composite was separated from the solution *via* centrifugation. The poly(AN-*co*-AMP)/BG dye composite was then suspended in 100 mL of 0.5 mol per L HCl solution and shaken for 60 minutes to regenerate BG dye from the polymer.

The produced dye-free poly(AN-*co*-AMP) was separated by centrifugation, washed several times with distilled water and dried for 24 h overnight. Finally, the dried free dye copolymer was subjected to another adsorption cycle.

3 Results and discussion

3.1. Synthesis of poly(AN-*co*-AMPS)

Poly(AN-*co*-AMPS) was prepared *via* a free radical copolymerization mechanism using KPS as an initiator in the presence of AN and AMPS monomers and water as the solvent. The polymerization was carried out in three main steps, namely, initiation, propagation and termination, as illustrated in Fig. 2. The initiation process begins with the homolytic cleavage of the persulfate anion into sulfate radicals ($SO_4^{\bullet -}$) under thermal conditions. These sulfate radicals act as strong oxidizing agents and react with AN and AMPS monomers, forming highly reactive monomeric radical species. These radicals act as active sites for subsequent polymer chain growth. During propagation, the radical sites continuously react with additional AN and AMPS monomers through a sequential chain-growth mechanism. This leads to the formation of alternating copolymer chains containing nitrile (–CN) and sulfonic acid ($-SO_3H$) functional groups. Finally, polymerization terminates when two growing polymer radicals recombine, forming a stable poly(AN-*co*-AMPS) copolymer. Another possible termination pathway is disproportionation, where two radicals transfer hydrogen atoms, leading to saturated and unsaturated polymer ends.

3.2. FTIR analysis

The FTIR spectra of the poly(AN-*co*-AMPS) copolymer before and after the adsorption process are shown in Fig. 3a. Starting with poly(AN-*co*-AMPS), the results exhibit two characteristic peaks at 2245.7 cm^{-1} and 2937 cm^{-1}, which are attributed to the stretching vibration of the nitrile group (C≡N) and the symmetrical and asymmetrical stretching vibration of C–H in CH_2, respectively.[38] These two characteristic peaks confirmed the AN unit. Moreover, the peak appears at 1045.23 cm^{-1} related to S=O in sulfonic acid group.[39] In addition, another peak appeared at 1635.34 cm^{-1} due to the stretching vibrations of (C=O) groups.[40] The characteristic peak at 1449.24 cm^{-1} was attributed to the bending vibration of the C–H group.[39] The C–S

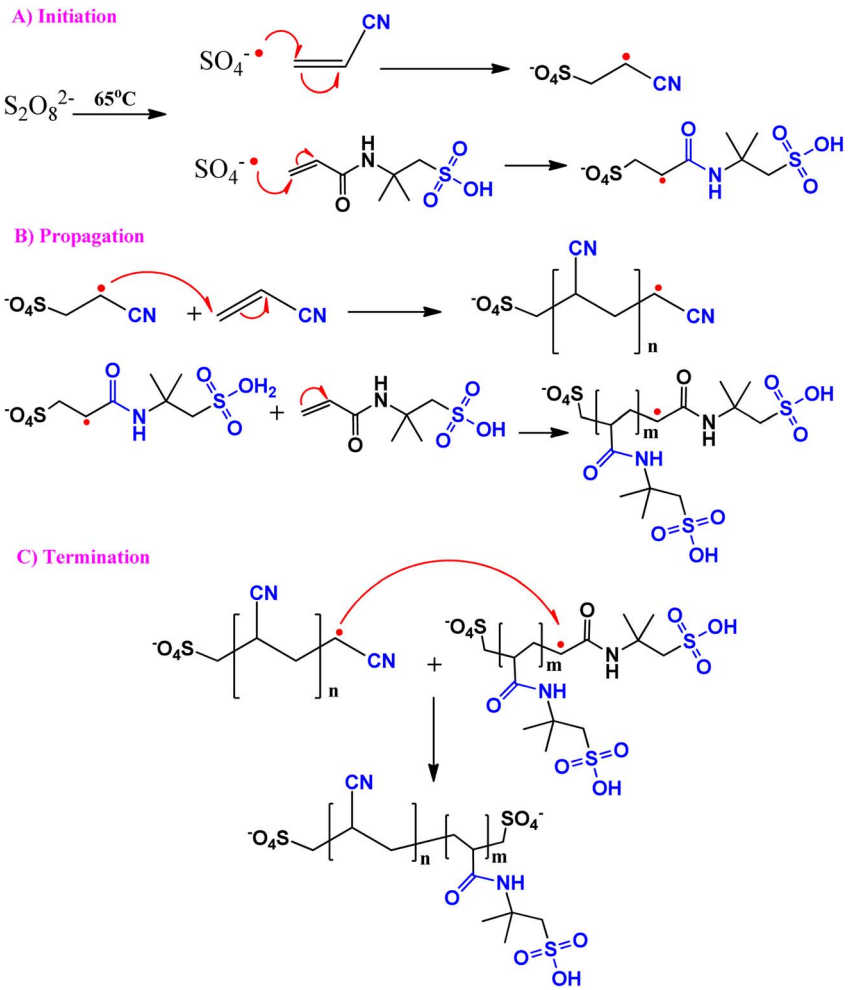

Fig. 2 Schematic of the free radical copolymerization mechanism of poly(AN-*co*-AMPS), illustrating the stages: (A) initiation, (B) propagation, and (C) termination.

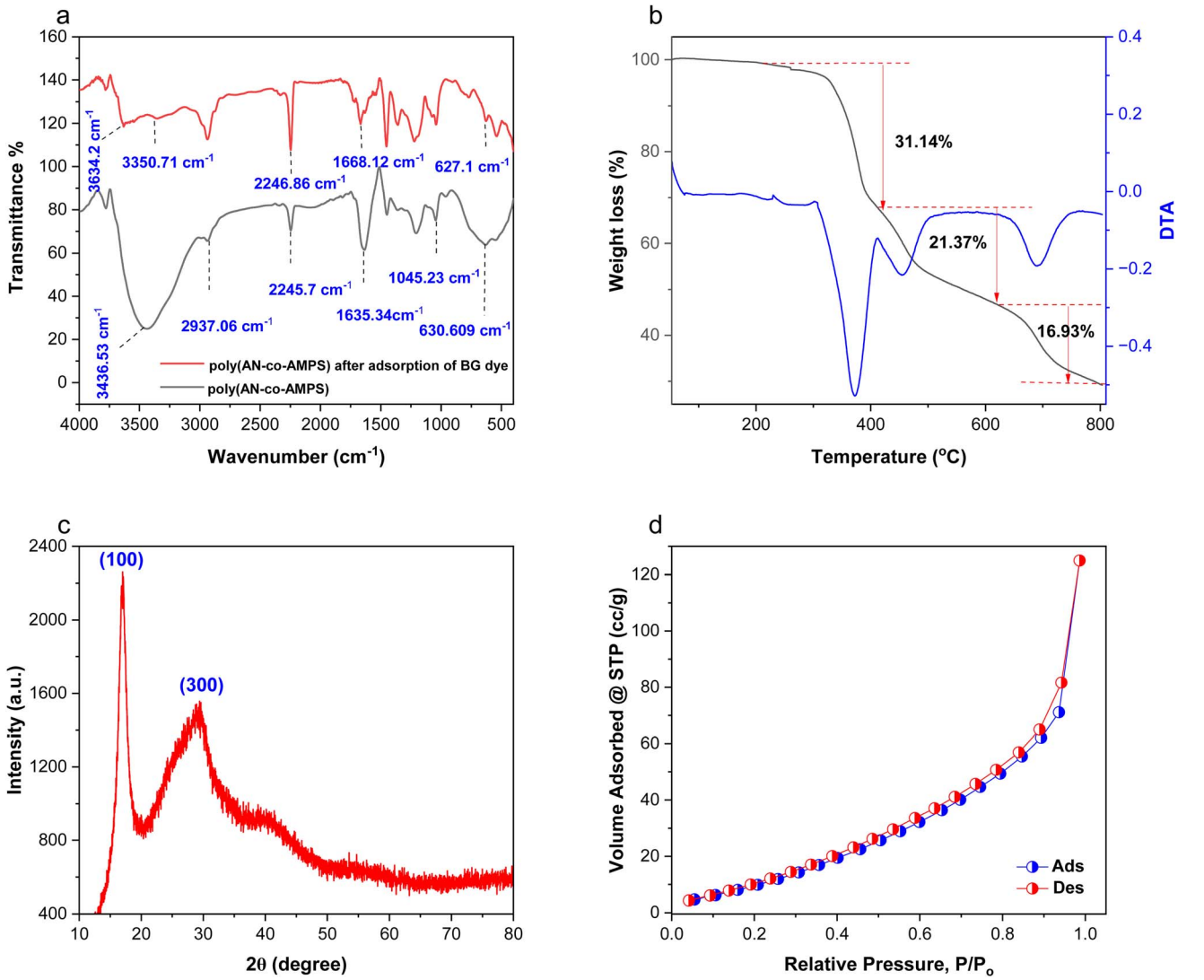

Fig. 3 FTIR spectra of poly(AN-*co*-AMPS) before and after adsorption (a); TGA analysis of poly(AN-*co*-AMPS) (b); XRD pattern of poly(AN-*co*-AMPS) (c); and N_2 adsorption–desorption isotherm of poly(AN-*co*-AMPS) (d).

stretching occurs at 630.609 cm^{-1}.[41] Furthermore, the broad peak at 3436.53 cm^{-1} is assigned to the NH and OH groups.[42] All these peaks confirmed the AMPS unit. Moving into poly(AN-*co*-AMPS) after adsorption experiments, it exhibits the same peaks of poly(AN-*co*-AMPS) before adsorption; however, the characteristic peaks of C=O shifted from 1635.34 cm^{-1} to appear at 1668.12 cm^{-1}. Moreover, the amide group band in poly(AN-*co*-AMPS) after the adsorption process was cleaved into two bands appearing at 335.71 cm^{-1} and 3634.2 cm^{-1}, and this change may be due to the interaction of NH amide groups in poly(AN-*co*-AMPS) with the BG dye. This observation confirms the interaction of the amide group of the copolymer with the BG dye.

3.3. Thermal properties of poly(AN-*co*-AMPS)

Thermal analysis was performed to examine the thermal stability of poly(AN-*co*-AMPS), as represented in Fig. 3b. According to the TGA curve, poly(AN-*co*-AMPS) demonstrated three degradation stages throughout the heating process. Initially, the degradation stage started from 304 °C to 411 °C with a weight loss equal to 31.14%. In this step, the weight loss can be attributed to the thermal breakdown of loosely held polymer chains at the polymer network's surface. The second step resulted in a weight loss equal to 21.37% at temperature range of 411–505 °C. This loss in weight can be attributed to the breakage of the polymer backbone chain. Finally, almost 16.93% of the sample mass was degraded in the range of 645–757 °C, which can be due to the complete decomposition of the polymer backbone.[43–45]

The activation energy (E^*) and Arrhenius constant (A') can be calculated using Coats–Redfern eqn (3):[46,47]

$$\log\left[\frac{-\log(1-\alpha)}{T^2}\right] = \log\left[\frac{A'R}{\theta E^*}\left(1-\frac{2RT}{E^*}\right)\right] - \frac{E^*}{2.303RT^*} \quad (3)$$

Table 1 Thermodynamic parameters of poly(AN-*co*-AMPS)

Stage	E^* (kJ mol^{-1})	A' (min^{-1})	ΔS^* (J mol^{-1} K^{-1})	ΔH^* (kJ mol^{-1})	ΔG^* (kJ mol^{-1})
1 at (304–411 °C)	89.89	778.9×10^3	−174.937	84.5441	197.0286
2 at (411–505 °C)	21.3107	1.34	−286.308	15.2831	222.856
3 at (645–757 °C)	45.762	24.460	−264.5007	37.7639	292.2136

where α is the fraction of sample decomposed at temperature T. θ is the heating rate and R is gas constant. By plotting $\log(-\log(1-\alpha)/T^2)$ against $1/T$, a straight line was produced (Fig. S1 in the ESI†). The value of activation energy was calculated from the slope and Arrhenius constant was calculated from the intercept. The entropy (ΔS^*), enthalpy (ΔH^*) and free energy of activation (ΔG^*) were determined using eqn (4)–(6).[48]

$$\Delta H^* = E^* - RT \quad (4)$$

$$\Delta S^* = 2.303R\left[\log\left(\frac{A'h}{K_B T}\right)\right] \quad (5)$$

$$\Delta G^* = \Delta H^* - T\Delta S^* \quad (6)$$

where h is the Planck constant and K_B is the Boltzmann constant. The results of activation energy, Arrhenius constant and thermodynamic parameters are represented in Table 1. The endothermic and nonspontaneous nature of the copolymer degradation is indicated by the positive values of ΔH^* and ΔG^*, respectively.

3.4. XRD analysis

The crystalline structure of the synthesized poly(AN-*co*-AMPS) copolymer was examined by X-ray diffraction (XRD) analysis and the relevant results are displayed in Fig. 3c and Table 2. As illustrated in Fig. 3c, the XRD pattern of poly(AN-*co*-AMPS) exhibits two distinct peaks at $2\theta = 16.944°$ and 29.488°, which corresponded to the (100) and (300) diffraction planes, respectively.[36,49,50] These two distinctive peaks confirm the crystalline structure of poly(AN-*co*-AMPS). In addition, the crystallite size (D) of the prepared poly(AN-*co*-AMPS) copolymer was calculated using the Scherrer eqn (7):[51]

$$D = \frac{K\lambda}{\beta\cos(\theta)} \quad (7)$$

where K is Scherrer's constant ($K = 0.89$), λ is the X-ray wavelength ($\lambda = 0.154$ nm), β is the full width at half maximum (FWHM) intensity and 2θ is Bragg's angle (peak position). After applying this equation to the peaks corresponding to poly(AN-*co*-AMPS), we are able to determine their average crystallite size and it is found to be equal to 1.4021 nm.

3.5. Brunauer–Emmett–Teller analysis (BET)

The specific surface area and pore volume of the produced poly(AN-*co*-AMPS) were assessed using BET analysis employing N_2 adsorption/desorption measurements at 77 K. The nitrogen adsorption/desorption isotherm of poly(AN-*co*-AMPS) is illustrated in Fig. 3d. The results show that poly(AN-*co*-AMPS) has a specific surface area equal to 64.0681 m^2 g^{-1} and that the

Table 2 XRD data of poly(AN-*co*-AMPS)

No.	2θ (°)	d value (Å)	Miller indices	Net intensity (counts)	Relative intensity (%)	Crystallite size (nm)	Average crystallite size (nm)
1	16.944	5.22855	(100)	1319.95	100	1.3863	1.4021
2	29.488	3.02668	(300)	772.820	58.5	1.4179	

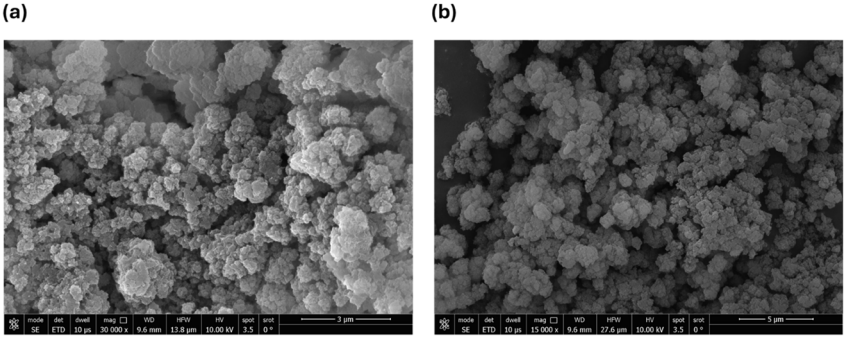

Fig. 4 FESEM images of poly(AN-*co*-AMPS) with different scales: 3 μm (a) and 5 μm (b).

adsorption/desorption curve fits type-IV isotherm. Moreover, it was found that the BJH pore volume and pore radius were measured at a saturated pressure to be equal to 0.196497 $cm^3\ g^{-1}$ and 1.66796 nm, respectively. Porous materials are categorized by the International Union of Pure and Applied Chemistry (IUPAC) according to their pore radius: macro-porous materials have a pore radius more than 50 nm, mesoporous materials have a pore radius between 2 and 50 nm and microporous materials have a pore radius less than 2 nm.[52] Therefore, poly(AN-*co*-AMPS) can be considered a microporous material. By comparing its surface area with that of other adsorbents reported in the literature, we found that poly(AN-*co*-

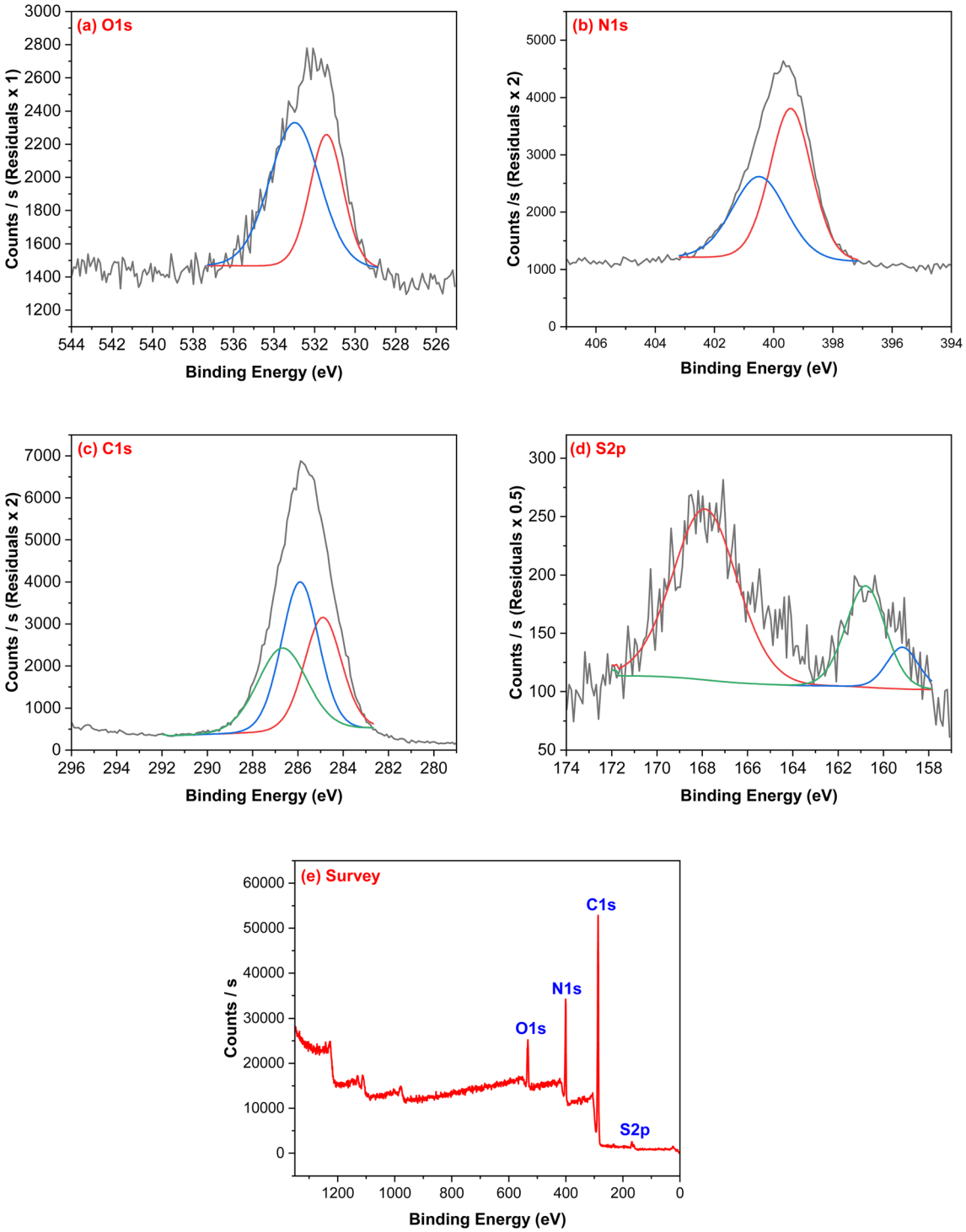

Fig. 5 XPS analysis of poly(AN-*co*-AMPS) copolymers: (a) high-resolution O 1s spectrum, (b) high-resolution N 1s spectrum, (c) high-resolution C 1s spectrum, (d) high-resolution S 2p spectrum, and (e) survey scan confirming the presence of C, N, O, and S elements in the copolymer structure.

AMPS) has a higher surface area than that of the other adsorbents, which enhances its removal efficiency.[13,53]

3.6. FESEM and EDX analysis

The surface morphology of the synthesized poly(AN-*co*-AMPS) copolymer was investigated by Field Emission Scanning Electron Microscopy (FESEM), and the obtained images are presented in Fig. 4. The FESEM micrographs at different magnifications reveal an aggregated, rough surface with a highly irregular texture. The observed morphology suggests a porous network, which is beneficial for adsorption applications as it enhances the surface area and provides active sites for dye molecule interaction. The qualitative elemental composition of poly(AN-*co*-AMPS) was clarified using EDX analysis. The chemical composition (in weight%) of poly(AN-*co*-AMPS) was reported by EDX analysis to be 55.43 for carbon, 6.30 for oxygen, 33.18 for nitrogen, and 1.39 for sulfur, as shown in Fig. S2 in the ESI.† Based on the sulfur content in poly(AN-*co*-AMPS), the ratio of AN to AMPS in copolymer was found to be 91/9.

3.7. XPS analysis

XPS analysis was performed to investigate the surface chemical composition and functional groups present in the synthesized poly(AN-*co*-AMPS). The wide-scan survey spectrum (Fig. 5e) confirms the presence of oxygen (O 1s), nitrogen (N 1s), carbon (C 1s), and sulfur (S 2p) at 533.72, 400.2, 287.48 and 167.13 eV, respectively, which are characteristic elements of the copolymer structure. The detailed high-resolution spectra of each element provide deeper insights into the functional groups present in the material. The C 1s spectrum (Fig. 5c) exhibits three major peaks at ~284.6 eV, 286.3 eV, and 288.2 eV, which correspond to the C–C/C=C, C–N/C–O, and C=O functional groups, respectively. These peaks confirm the presence of AN and AMPS units in the copolymer backbone. The N 1s spectrum (Fig. 5b) displays a peak at ~399.5 eV, attributed to the nitrile (–C≡N) and amide (–NH) groups from the AN and AMPS monomers, respectively. The presence of nitrogen further supports the successful incorporation of these monomers into the polymer structure. The O 1s spectrum (Fig. 5a) contains two peaks at ~531.2 eV and 532.8 eV, corresponding to oxygen in the amide ($–CONH_2$) and sulfonic acid ($–SO_3H$) functional groups, respectively. The S 2p spectrum (Fig. 5d) confirms the presence of sulfonic acid ($–SO_3H$) groups, with peaks at ~168.5 eV and 169.8 eV. The presence of sulfur verifies the successful incorporation of AMPS into the copolymer structure. Overall, the XPS analysis confirms the successful synthesis of poly(AN-*co*-AMPS), highlighting its rich functional groups (nitrile, amide, and sulfonic acid) that can contribute to the adsorption of BG dye.

3.8. Adsorption batch experiment

3.8.1. Effect of contact time. The contact time varied from 5 to 120 min, while the other parameters such as adsorbent

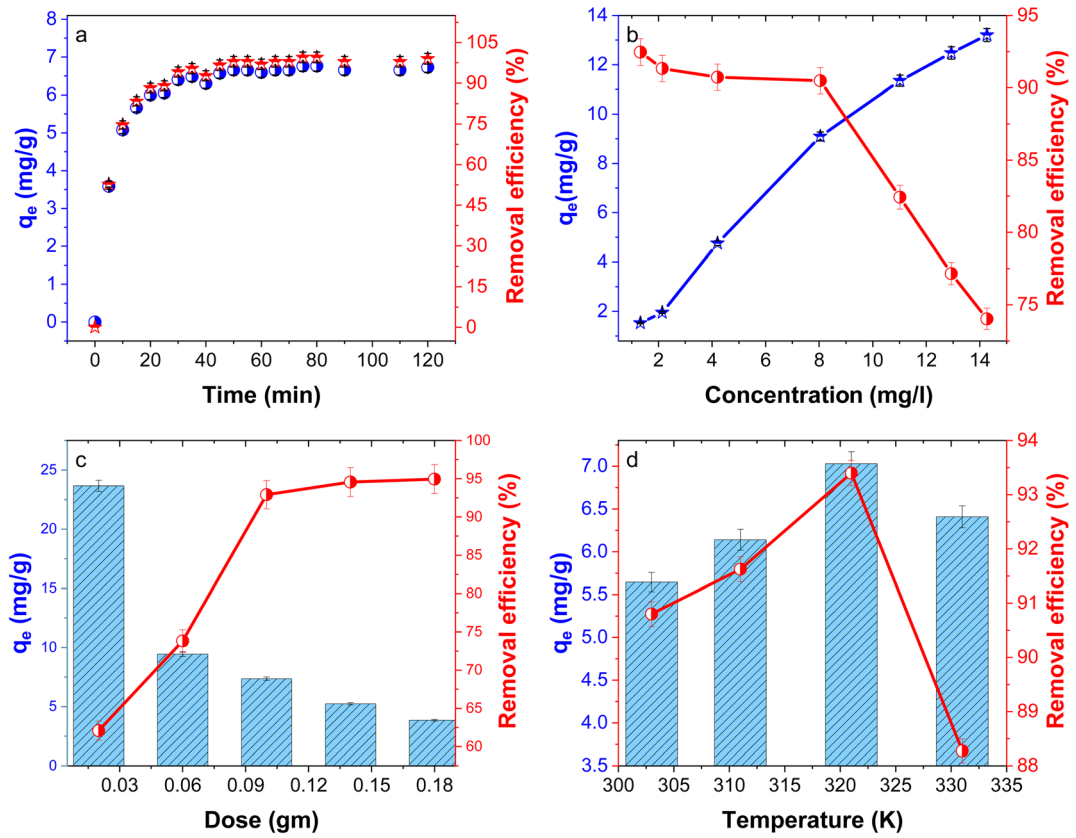

Fig. 6 Effect of contact time on the adsorption of BG onto poly(AN-*co*-AMPS) (a); effect of initial concentration of BG on adsorption process (b); effect of poly(AN-*co*-AMPS) dose on the adsorption of BG dye (c); and effect of temperature on BG adsorption onto poly(AN-*co*-AMPS) (d).

dosage, initial concentration of BG dye, temperature, pH and shaking rate were maintained constantly. The effect of contact time on the adsorption of BG dye is shown in Fig. 6a. The figure demonstrates that the removal efficiency (%R) and adsorption capacity (q_e) of BG dye on poly(AN-*co*-AMPS) steadily increase with the increase in contact time by a higher rate up to about 40 min and then the adsorption process occurred at a lower rate, and finally, an equilibrium was achieved. This behavior can be understood by two reasons: the first one is the presence of many adsorption sites on the polymer surface in the beginning of adsorption process that can be interacted with the BG dye, so that the adsorption process initially occurred at a higher rate. As the adsorption process progresses, these sites are occupied with dye molecules, which lead to diminishing adsorption until equilibrium is established.[54] The second reason could be the effect of mass transfer of dye molecules from bulk solution to adsorbent surface. As the adsorption process progresses, the concentration of dye molecules decreases, which leads to diminishing mass transfer number, as well as a decrease in the diffusion rate and the adsorption process.[55]

3.8.2. Effect of dye concentration. The effect of initial dye concentration on the adsorption of BG dye using poly(AN-*co*-AMPS) is presented in Fig. 6b As we can see, increasing the BG dye concentration from 1.3 to 14.3 mg L^{-1} leads to a decrease in dye removal percentage (%R) from 92.46 to 74.02, while the amount of BG dye adsorbed per one gram adsorbent (q_e) increased from 1.529 to 13.203 mg g^{-1}. The decrease in %R is attributed to the higher concentration of BG dye molecules in the solution, which increases the competition for available adsorption sites. Once these sites are saturated, excess dye remains in the solution, reducing the overall removal percentage.[56,57] However, the increase in q_e value could be attributed to the ability of adsorbents to absorb more dye per unit mass as the concentration of dye increases, up until it reaches its maximum capacity. This is because the adsorbent has more opportunities to interact with and collect dye molecules when there is more dye accessible in the solution.[58]

3.8.3. Effect of adsorbent dose. The effect of dose of poly(AN-*co*-AMPS) on the adsorption of BG dye was investigated by adding various amounts of poly(AN-*co*-AMPS) from 0.02 to 0.18 g to the BG dye solution (100 mL, 7.5 mg L^{-1}) at room temperature and at pH = 7 for 1 hour, and the relevant results are represented in Fig. 6c. When the adsorbent dose is increased, the removal efficiency of BG dye increases from 62.08732% to 94.952%. This behavior is attributed to the increase in adsorbent surface area or the availability of more adsorption sites that are able to interact or capture dye molecules.[59] However, the adsorption capacity reduces from 23.66 to 3.85 mg g^{-1} as the dose of poly(AN-*co*-AMPS) increases due to the decrease in adsorbate-to-adsorbent ratio.[58]

3.8.4. Effect of temperature. The experiments were conducted at different temperatures ranging from 303 to 331 K, but the other parameters such as contact time, adsorbent dosage, initial concentration of BG dye, pH and shaking rate were keeping constant. The influence of temperature on the adsorption of BG dye is represented in Fig. 6d. The results indicate that, by increasing the temperature from 303 to 321 K, both the removal percentage and the adsorption capacity of the BG dye were increased from 90.8% to 93.4% and from 5.65 to 7.03 mg g^{-1}, respectively. After that, increasing the temperature above 321 K diminishes both values of %R and q_e to 88.27 and 6.407 mg g^{-1}, respectively. The increasing behavior can be attributed to the increase in the kinetic energy with the increase in temperature that allows BG dye molecules to move faster and collide with poly(AN-*co*-AMPS) by a higher rate, and finally, enhances the adsorption process. In addition, the higher temperatures could improve the adsorption capacity of the poly(AN-*co*-AMPS) through overcoming the energy barriers related to BG dye molecules to interact with the adsorbent sites of the polymer. Moreover, the increase in temperature enhances the diffusion of BG dye molecules from the bulk solution to the adsorbent surface; as a result, the BG dye is removed from the solution at a higher rate.[60] Moving into the decreasing behavior, the continued increase in adsorption temperature leads to saturating the adsorption sites at poly(AN-*co*-AMPS). At this

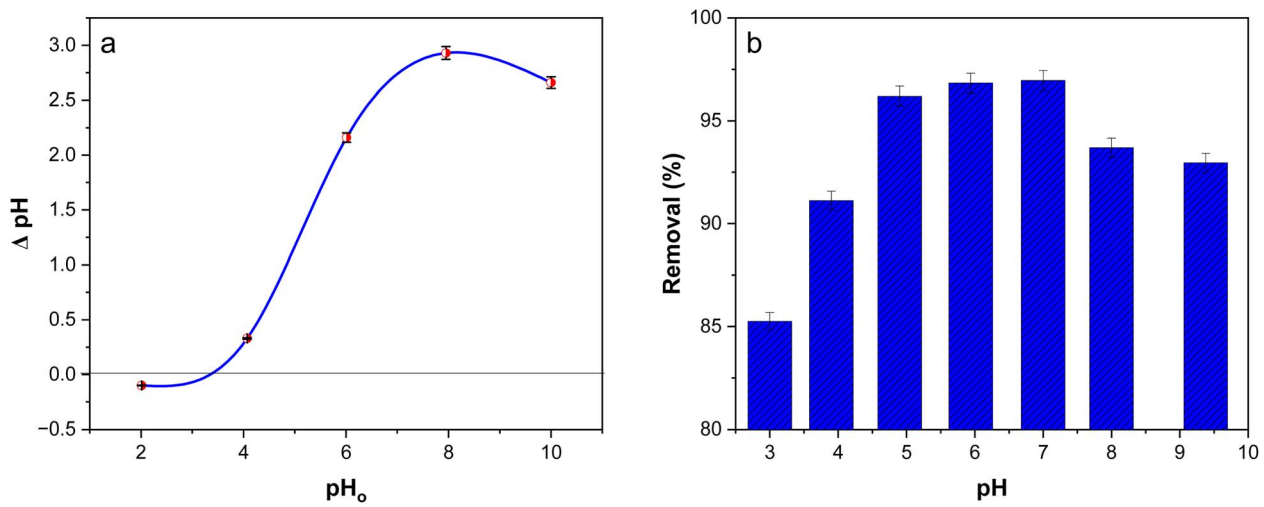

Fig. 7 PCZ of poly(AN-*co*-AMPS) (a) and effect of pH on the adsorption of BG onto poly(AN-*co*-AMPS) (b).

point, more increases in temperature will enhance the kinetic energy that motivates the desorption of dye molecules from the poly(AN-*co*-AMPS) surface. Moreover, high temperatures could disrupt the adsorption equilibrium by favoring desorption over adsorption.[60]

3.8.5. Point of zero charge (PZC). PZC is the value at which all active sites remain neutral, and the material's surface charge becomes zero. The PZC of poly(AN-*co*-AMPS) was calculated by preparing 25 mL of 0.1 M KNO_3 solutions with different pH values in the range of 3–9. The pH of each solution was adjusted with 0.1 M NaOH and 0.1 M HCL solution and monitored using a pH meter. Then, 0.05 g of copolymer was added into each solution. After that, the bottles were shaken for 24 h at room temperature and the final pH values of the solutions were determined; then, the PZC of poly(AN-*co*-AMPS) was calculated. The point of zero charge curve is represented in Fig. 7a. The figure indicates that the PZC of poly(AN-*co*-AMPS) was determined to be $pH_{pzc} = 3.4$. At a pH below this PZC, the surface of poly(AN-*co*-AMPS) becomes positively charged, which is favorable for removing anionic dyes. However, at a pH higher than 3.4, the surface of poly(AN-*co*-AMPS) gained negative charges that are favorable for removing cationic dyes.

3.8.6. Effect of pH. To investigate the effect of pH on the BG dye adsorption, the experiments were carried out in the pH range of 3 to 9 with 7.5 mg L^{-1} dye concentration, 0.1 g from adsorbent and shaking for 1 hour. The results of the experiments are shown in Fig. 7b. The removal percentage of BG dye increased with the increase in pH value from 3 to 7, while the percentage of removal of BG dye decreased as the pH increased above 7. The maximum percentage of removal was found to be 96.8 at pH 7 and then it gradually decreased. The reason for this behavior is that BG dye is a cationic dye that stays as positively charged in solutions as well as the concentration of H^+ is high at a lower pH value, so that protons can be adsorbed competitively with the BG dye on the surface of poly(AN-*co*-AMPS) and lower the BG dye adsorption.[1,14] In addition, more negatively charged adsorption sites become available at higher pH values. The removal percentage increases as a result of the adsorbent site' electrostatic attraction to the dye molecules.[61] However, at a pH more than 7, BG molecules undergo competitive interactions with the amide group (–OH, $–NH_2$) and sulfonic group on the surface of copolymers and free OH ions present in the medium lead to a decrease in the BG dye adsorption.[61] Thus, the optimum pH for remaining adsorption experiments was chosen as 7 for the BG dye.

3.8.7. Effect of ionic strength. The effect of ionic strength on the adsorption of BG dye onto poly(AN-*co*-AMPS) was investigated by varying the NaCl concentration from 0 to 0.5 mol L^{-1} while keeping other parameters such as initial dye concentration, adsorbent dosage, pH, and temperature constant. The results are presented in Fig. 8, which shows a noticeable decline in dye removal efficiency from 100% to 58% as the NaCl concentration increases. This reduction in adsorption efficiency can be attributed to the shielding effect of electrostatic interactions at higher ionic strengths. The increased concentration of Na^+ ions in the solution competes with the cationic dye molecules for active adsorption sites, leading to charge

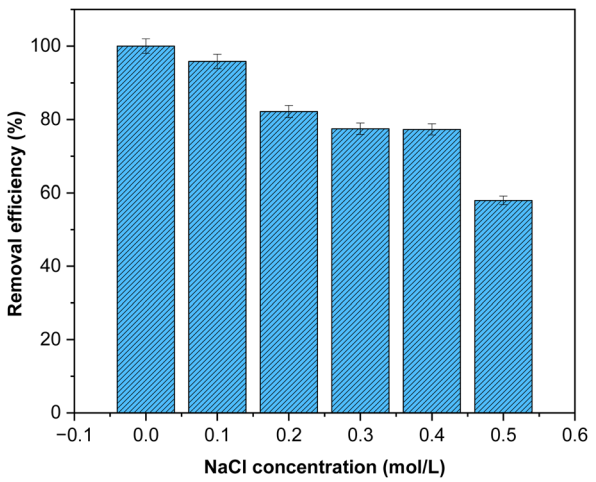

Fig. 8 Effect of ionic strength on the adsorption of BG onto poly(AN-*co*-AMPS).

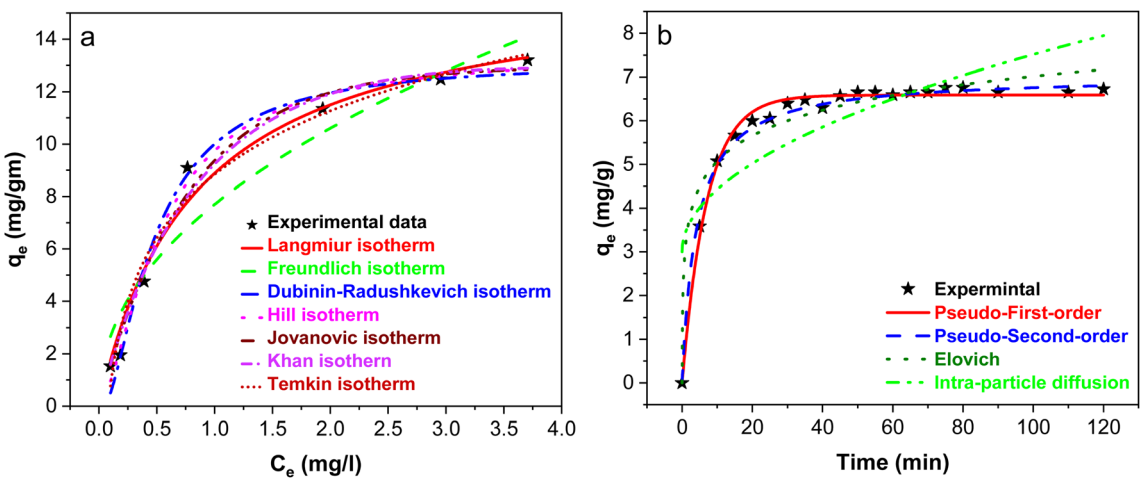

Fig. 9 Adsorption isotherms of BG onto poly(AN-*co*-AMPS) (a) and adsorption kinetic models of BG onto poly(AN-*co*-AMPS) (b).

neutralization on the polymer surface. Consequently, the electrostatic attraction between the adsorbent and dye is weakened, resulting in a lower adsorption capacity. These findings highlight the significance of ionic strength in practical wastewater treatment applications, where competing ions may influence the adsorption performance. This reduces the electrostatic attraction between the adsorbent and dye, leading to lower dye removal efficiency.[62,63]

3.9. Adsorption isotherms

Adsorption isotherms are an important method that helps in describing the interactions between the adsorbent and the adsorbate, as well as in investigating the adsorption mechanisms. Several adsorption isotherms have been used to clarify the type of isotherm, reaction nature whether monolayer or multilayer adsorption, adsorbent affinity, adsorption mechanism and maximum adsorption capacity. Seven models were used to fit the experimental data including Langmuir, Freundlich, Dubinin–Radushkevich (D–R), Temkin, Khan, Jovanovic, and Hill isotherm.[64–67]

The non-linear representation of all mentioned adsorption isotherm models is presented in Fig. 9a, and their corresponding calculated outcomes are summarized in Table 3. The Langmuir model is applied to monolayer adsorption on homogeneous sites, whereas the Freundlich model suites are applied to multilayer adsorption on heterogeneous sites. According to the data in Table 3, the experimental results exhibit a better linear fit toward Langmuir ($R^2 = 0.97566$) rather than Freundlich ($R^2 = 0.91287$), which suggests that the adsorption sites on poly(AN-*co*-AMPS) are uniform and the adsorption of BG dye molecules occurred by the monolayer adsorption form without any interactions between the adsorbed BG dye molecules. Moreover, poly(AN-*co*-AMPS) achieved a maximum adsorption capacity (q_m) by Langmuir as 16.28 mg g^{-1}, which is larger than q_m achieved by other adsorbents reported in the literature.[11,26,56] The D–R isotherm was created by

Table 3 Adsorption isotherm of BG onto poly(AN-*co*-AMPS)[a]

Isotherm	Equation	Value of parameters	
Langmuir	$q_e = \frac{K\, q_m C_e}{1 + KC_e}$	q_m (mg g^{-1})	16.28863
		K (L mg^{-1})	1.20016
		R-Square (COD)	0.97972
		R^2	0.97566
Freundlich	$q_e = KC_e^{1/n}$	K (mg g^{-1})	7.69999
		$1/n$	0.46152
		R-Square (COD)	0.9274
		R^2	0.91287
Dubinin–Radushkevich	$q_e = q_m e^{-K\varepsilon^2}$	q_m (mg g^{-1})	13.11347
	$\varepsilon = \left[RT \ln\left(1 + \frac{1}{C_e}\right)\right]$	k (mol^2 J^{-2})	3.73×10^{-9}
	$E_a = \frac{1}{\sqrt{2K}}$	E_a (kJ mol^{-1})	11.576
		R-Square (COD)	0.98707
		R^2	0.984044
Temkin	$q_e = B \ln(KC_e)$	B	3.50068
		K	12.49605
		R-Square (COD)	0.975
		R^2	0.97
Khan	$q_e = \frac{(q_m KC_e)}{((1 + kC_e)^n)}$	q_m (mg g^{-1})	33.21503
		k	0.51871
		n	1.49227
		R-Square (COD)	0.98393
		R^2	0.97589
Jovanovic	$q_e = q_m(1 - e^{-KC_e})$	q_m (mg g^{-1})	12.95886
		k	1.28322
		R-Square (COD)	0.98538
		R^2	0.98246
Hill	$q_e = \frac{(q_m C_e^n)}{(K + C_e^n)}$	q_m (mg g^{-1})	13.52877
		k	0.38869
		n	1.52645
		R-Square (COD)	0.9917
		R^2	0.98755

[a] In this table, q_e (mg g^{-1}) is the adsorption capacity of poly(AN-*co*-AMPS) at equilibrium, q_m is the maximum adsorption capacity (mg g^{-1}), C_e is the equilibrium concentration (mg L^{-1}), K is a rate constant, n in the Freundlich model is the number of layers, B (J mol^{-1}) is the Temkin constant related to the heat of adsorption, E_a (kJ mol^{-1}) is the adsorption free energy, R (J mol^{-1} K^{-1}) is the general gas constant and T (K) is the absolute temperature.

adapting the Polanyi potential theory of adsorption. It is applied on microporous adsorbents and assumes the pores in the adsorbent obey Gaussian energy distribution. In addition, it helps to distinguish between chemisorption and physisorption processes according to the value of adsorption free energy (E_a). The physisorption process exhibits an E_a value less than 8 kJ mole^{-1}, while the chemisorption process exhibits an E_a value greater than 8 kJ mole^{-1}.[68] Appling the mathematical equation of (D–R) isotherm on the experimental data of adsorption of BG dye on poly(AN-*co*-AMPS) appears a good fitting with a high R^2 value equal to 0.984044. Moreover, the calculated value of adsorption free energy was found to be 11.576 kJ mol^{-1}, which strongly suppose that the adsorption of BG dye is chemisorption on microporous poly(AN-*co*-AMPS). The Temkin isotherm model is mainly based on the linear decrease in adsorption energy with the increase in the coverage of the adsorbent surface rather than decrement exponentially, as proposed by the Freundlich isotherm model. The adsorbent saturation after the completion of the adsorption process is also taken into account. The Khan isotherm is useful for explaining the behavior of adsorption in systems with relatively high solute concentrations. The Jovanovic isotherm built upon the assumptions based on the Langmuir isotherm model with few possible inclusions of mechanical contact among the desorbing and adsorbing molecules. The adjustment of the adsorption surface from this model made the equation less effective in the physical adsorption but can be applied to adsorption with both mobile and localized monolayers without lateral interaction. Moreover, at high concentrations, the adsorption reaches saturation, whereas at low concentrations, it follows Henry's law.

3.10. Adsorption kinetics

The adsorption kinetics is often an important class to illustrate the adsorption mechanism. Different kinetic models have been used to investigate the adsorption mechanism and rate-controlling steps in adsorption processes. In this work, the experimental data were analyzed by the pseudo-first-order (PFORE), pseudo-second-order (PSORE), intra-particle diffusion (IPD), and Elovich kinetic models.[65,69,70] PFORE assumed that the adsorption process rate is directly proportional to the number of unoccupied sites on the adsorbent surface, while PSORE supposed that the process of adsorption is controlled by chemisorption mechanism through transferring or sharing of electrons between the adsorbent and the adsorbate surface.[65] Fig. 9b illustrates the plot of q_t against time for all models. Moreover, the kinetic parameters and correlation coefficients (R^2) are presented in Table 4. By comparing the correlation coefficients (R^2) displayed in Table 4 for both PFORE and PSORE models, we found that the data exhibit a better linear fit (R^2 value) for PSORE than for PFORE, which indicates that the pseudo-second-order model is more appropriate for describing the adsorption process. Moreover, the mechanism of the adsorption of BG onto poly(AN-*co*-AMPS) and the rate limiting steps were further studied by the IPD model. According to the assumption of the IPD model, the adsorption process may be controlled by one or more steps, for example, film diffusion, bulk diffusion and intra-particle diffusion or combination of more than one step. Fig. 9b shows that the adsorption capacity produces a linear relationship with the square root of time, which indicates that the system is governed by intra-particle diffusion only. The differentiable chemisorption of BG onto poly(AN-*co*-AMPS) was assessed using the Elovich model. Based on the results in Fig. 9b and Table 4, the high value of R^2 confirms the model's appropriateness. The results of this study indicate that BG adsorption onto poly(AN-*co*-AMPS) occurs

Table 4 Adsorption kinetics of BG onto poly(AN-*co*-AMPS)[a]

Model	Equation	Value of parameters	
Pseudo-first order	$q_t = q_e(1 - e^{K_1 t})$	q_e (mg g^{-1})	6.58978
		K_1 (min^{-1})	0.14143
		R-Square (COD)	0.99094
		R^2	0.99043
Pseudo-second order	$q_t = \frac{(q_e^2 K_2 t)}{(1 + q_e K_2 t)}$	q_e (mg g^{-1})	7.09706
		K_2 (g mg^{-1} min^{-1})	0.03372
		R-Square (COD)	0.9955
		R^2	0.99405
Elovich	$q_t = \frac{1}{\ln(\alpha\beta t + 1)}$	β (g mg^{-1})	1.18442
		α (mg g^{-1}.min)	34.33037
		R-Square (COD)	0.96011
		R^2	0.9579
Intra-particle diffusion	$q_t = K_{diff} t^{0.5} + C$	K_{diff} (mg g^{-1} min$^{-1/2}$)	0.45159
		C	3.0013
		R-Square (COD)	0.63632
		R^2	0.61612

[a] In this table, q_e (mg g^{-1}) and q_t (mg g^{-1}) are the adsorption capacities of poly(AN-*co*-AMPS) at equilibrium and at time t, respectively, K_1 (min^{-1}) and K_2 (g mg^{-1} min^{-1}) are the rate constants of pseudo-first-order and pseudo-second-order adsorption, respectively, k_{diff} (mg g^{-1} min$^{-1/2}$) is the rate constant of intra-particle diffusion, α (mg g^{-1} min^{-1}) is the initial sorption rate, and β (g mg^{-1}) is related to the extent of surface coverage and activation energy for chemisorption.

according to chemisorption kinetics and that the Elovich equation can accurately describe this process.

3.11. Adsorption thermodynamics

In order to describe the adsorption nature of BG on poly(AN-*co*-AMPS), several thermodynamic parameters such as the Gibbs free energy change (ΔG), change of entropy (ΔS) and enthalpy change (ΔH) were evaluated. They are calculated depending on the experimental data obtained at a temperature in the range of 303 K to 321 K using van't Hoff equations as follows:

$$K = \frac{C_{AC}}{C_e} \tag{8}$$

$$\ln K = \frac{\Delta S}{R} - \frac{\Delta H}{RT} \tag{9}$$

$$\Delta G = \Delta H - T\Delta S \tag{10}$$

where R is the universal gas constant (8.314 J mol^{-1} K^{-1}), T is the absolute temperature in kelvin, K is the standard thermodynamic equilibrium constant, C_e is the equilibrium concentration of BG dye in solution (mg L^{-1}) and C_{AC} is the amount of BG adsorbed on the adsorbent at equilibrium (mg L^{-1}).

The plot of ln K_c against 1/T is represented in Fig. 10. (ΔS) and (ΔH) were calculated from the intercept and the slope of plot in the Fig. 10. The Gibbs free energy was calculated using eqn (10). All the values of thermodynamic parameters are represented in Table 5. The endothermic and spontaneous nature of BG adsorption is indicated by the positive ΔH and negative ΔG values, and this is further supported by the observation that the ΔG values decrease with the increase in temperature. The positive ΔS value indicates an increase in disorder at the solid–solution interface during the adsorption of BG dye onto poly(AN-*co*-AMPS).

3.12. Adsorption mechanism

The adsorption of BG dye onto the synthesized poly(AN-*co*-AMPS) copolymer is primarily driven by multiple interaction mechanisms including electrostatic interactions, π–π interactions, and hydrogen bonding, as illustrated in Fig. 11. The copolymer contains sulfonate (–SO_3^-) groups from AMPS, which contribute to its negatively charged surface. Since the BG dye is cationic, a strong electrostatic attraction occurs between the negatively charged sulfonate groups of the polymer and the positively charged quaternary ammonium groups of the dye molecules.[71] Additionally, the π–electron systems from the nitrile (–C≡N) groups can interact with the aromatic rings present in BG dye molecules *via* π–π stacking interactions, which further enhance the adsorption efficiency.[72] Furthermore, the presence of amide (–CONH–) and sulfonate (–SO_3H) functional groups in the copolymer allows for the formation of hydrogen bonds with BG dye molecules.[13] The amide group can act as both a hydrogen bond donor and an acceptor, contributing to the stabilization of the adsorbed dye molecules on the polymer matrix. Such interactions are particularly significant in stabilizing the dye–polymer complex, increasing the overall adsorption capacity.

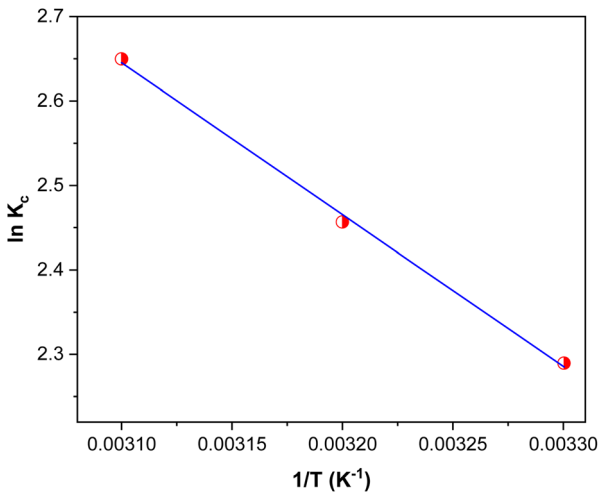

Fig. 10 Plot of ln K_c against 1/T for BG dye adsorption onto poly(AN-*co*-AMPS).

Table 5 Thermodynamic parameters of the adsorption of BG onto poly(AN-*co*-AMP)

	Parameters		
Temperature (K)	ΔG (kJ mol^{-1})	ΔH (kJ mol^{-1})	ΔS (J mol^{-1} K^{-1})
303	−20.6880	14.946	68.326
311	−21.2346		
321	−21.9179		

3.13. Regeneration study

In order to evaluate the reusability and stability of poly(AN-*co*-AMPS) as a sustainable adsorbent for removing BG dye from the aqueous solution, an adsorption/desorption experiment was conducted in six cycles and the results are presented in Fig. 12a. As we can notice that there is no decrease in the removal efficiency with the increase in adsorption–desorption cycles. In addition, to check the wellness adsorbent, the stability of the desorbed copolymer was characterized by FTIR spectroscopic analysis. The FTIR spectra of poly(AN-*co*-AMPS) before and after the regeneration experiments are shown in Fig. 12b. This figure shows that all peaks related to the functional groups of poly(AN-*co*-AMPS) did not change after recycling for six cycles. These results validate and demonstrate the relative efficiency, high reusability, stability and high application potential of poly(AN-*co*-AMPS) for removing BG dye under the experimental conditions. In addition to its high adsorption efficiency and reusability, the long-term sustainability of poly(AN-*co*-AMPS) as an adsorbent is a crucial consideration. The synthesis process utilizes cost-effective and readily available monomers, making large-scale production economically feasible. Furthermore, the recyclability of the copolymer, as demonstrated in the regeneration experiments, reduces the need for frequent replacement, thereby minimizing waste. Moreover, the copolymer's low-toxic nature and stability suggest its potential for environmentally friendly applications.

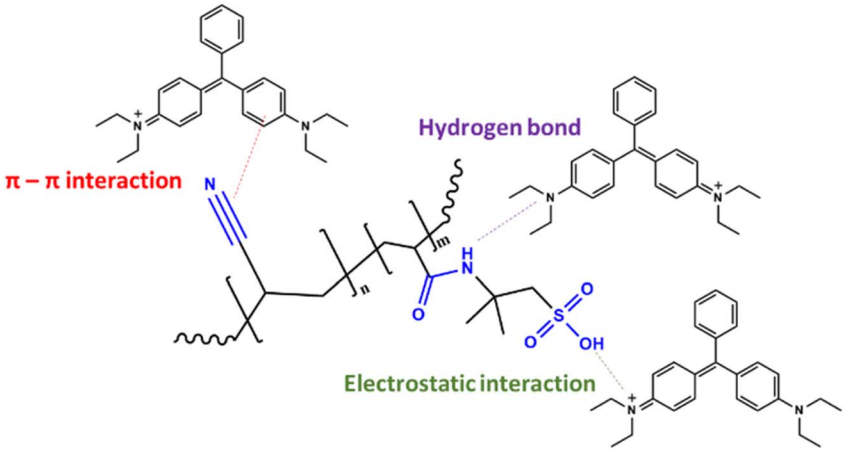

Fig. 11 Schematic of the interaction mechanisms between poly(AN-*co*-AMPS) and BG dye.

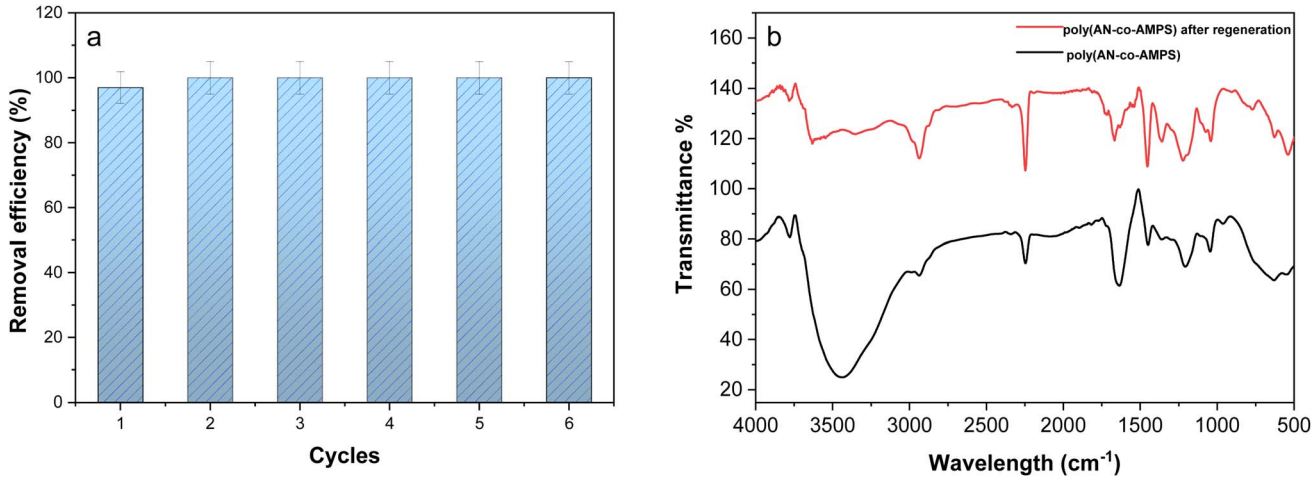

Fig. 12 Regeneration efficiency of poly(AN-*co*-AMPS) for the adsorption of BG (a) and IR spectra of poly(AN-*co*-AMPS) before and after regeneration experiment (b).

3.14. Statistical analysis of process optimization

3.14.1. Box–Behnken design (BBD). The BBD tool was used to analyze different variable interactions. We used the BBD in this work because it is easy to use, helps to reduce the number of experiments and provides a more accurate prediction of the response.[65] The designed experiment included 17 experiments, and the adsorption capacity (q_e) was considered as the response surface to the variables. Table 6 presents the results of the experiments conducted using the BBD, and the obtained and predicted adsorption capacity. Eqn (11) provides an explanation of the quadratic equation model:

$$q_e = +3.84 + 0.5813 \times A - 3.79 \times B + 2.50 \times C - 0.9173 \times AB + 0.1901 \times AC - 0.139 \times BC - 0.5547 \times A^2 + 2.18 \times B^2 + 0.1767 \times C^2 \quad (11)$$

It is possible to predict the reaction for specific levels of each element by using the equation expressed in terms of coded factors eqn (11). The factors' high levels are automatically written as +1 and their low levels as −1. By comparing the factor coefficients, the coded equation can be used to determine the relative impact of the components.

Eqn (12) may be used to represent the actual equation:

$$q_e = +3.79785 + 0.046062 \times \text{time} - 0.076989 \times \text{dose} + 0.700907 \times \text{concentration} - 0.000199 \times \text{time} \times \text{dose} + 0.000661 \times \text{time} \times \text{concentration} - 0.003481 \times \text{dose} \times \text{concentration} - 0.000168 \times \text{time}^2 + 0.000341 \times \text{dose}^2 + 0.007069 \times \text{concentration}^2 \quad (12)$$

For specific amounts of each factor, predictions regarding the reaction can be made using the equation expressed in terms of the actual factors. In this case, each factor's levels ought to be stated in their original units. This equation is not to be used to choose the relative impact of each factor because the coefficients are scaled to suit the units of each factor and the intercept not at the point of the design space.

Table 6 Results of the adsorption capacity of poly(AN-*co*-AMPS)

	Factors			q_e (mg g^{-1})		
Run	Time (min)	Dose (mg)	Concentration(mg L^{-1})	Experimental	Predicted	Residual
1	120	100	2.5	1.17682	1.35	−0.1725
2	120	180	7.5	2.11468	1.33	0.7811
3	62.5	100	7.5	3.83707	3.84	3.36×10^{-7}
4	5	180	7.5	2.02736	2.01	0.0218
5	62.5	100	7.5	3.83707	3.84	3.36×10^{-7}
6	62.5	20	12.5	14.4896	13.88	0.6087
7	5	20	7.5	6.97651	7.76	−0.7811
8	120	100	12.5	6.1447	6.73	−0.5868
9	62.5	180	2.5	0.68360	1.29	−0.6087
10	5	100	12.5	5.36116	5.19	0.1725
11	62.5	180	12.5	3.31532	3.51	−0.1943
12	62.5	100	7.5	3.83707	3.84	-2.24×10^{-7}
13	5	100	2.5	1.1538	0.5670	0.5868
14	120	20	7.5	10.7331	10.75	-2.24×10^{-7}
15	62.5	100	7.5	3.83707	3.84	-2.24×10^{-7}
16	62.5	100	7.5	3.83707	3.84	-2.24×10^{-7}
17	62.5	20	2.5	6.28866	6.09	0.1943

Analysis of variance (ANOVA) was carried out for the adsorption of BG onto poly(AN-*co*-AMPS) to identify key elements and interactions that affect the adsorption of BG and to demonstrate the relevant criteria in certified modeling. ANOVA was also used to define the interactions between process and response variables through graphical data analysis. The ANOVA results for the response surface experimental are presented in Table 7. The *P*-value helps determine whether adding additional terms to the model significantly improves the fit. A *p*-value less than 0.05 indicates that the added terms contribute meaningfully to the model. As can be seen in Table 8, the high quantities of the *F*-value ($F = 55.91$) and the smaller *P*-value ($p < 0.05$) denote the significance of the applied model. The coefficient of determination (R^2) quantifies the proportion

Table 7 ANOVA results for response surface

Source	Sum of square	df	Mean square	*F*-Value	*P*-Value	Remark	Standard error	95% CI low	95% CI high
Intercept							0.2821	3.17	4.50
Model	200.26	9	22.25	55.91	<0.0001	Significant			
A-Time	2.70	1	2.70	6.79	0.0351		0.2230	0.05	1.11
B-Dose	115.12	1	115.12	289.24	<0.0001		0.2230	−4.32	−3.27
C-Concentration	50.04	1	50.04	125.73	<0.0001		0.2230	1.97	3.03
AB	3.37	1	3.37	8.46	0.0227		0.3154	−1.66	−0.171
AC	0.1446	1	0.1446	0.3633	0.5657		0.3154	−0.555	0.9360
BC	7.75	1	7.75	19.48	0.0031		0.3154	−2.14	−0.646
A^2	1.30	1	1.30	3.25	0.1142		0.3075	−1.28	0.1723
B^2	20.02	1	20.02	50.30	0.0002		0.3075	1.45	2.91
C^2	0.1315	1	0.1315	0.3304	0.5834		0.3075	−0.550	0.9037
Residual	2.79	7	0.3980						
Lack of fit	2.79	3	0.9287						
Pure error	0.0000	4	0.0000						
Cor total	203.05	16							

Table 8 Statistical summary of different models of adsorption of BG onto poly(AN-*co*-AMPS)

Source	Std. dev.	Sequential *p*-value	Press	R^2	Adjusted R^2	Predicted R^2	Remark
Linear	1.65	<0.0001	70.19	0.8267	0.7867	0.6543	
2FI	1.55	0.2575	108.50	0.8822	0.8115	0.4657	
Quadratic	**0.6309**	**0.0012**	**44.58**	**0.9863**	**0.9686**	**0.7805**	**Suggested**
Cubic	3.039×10^{-7}	<0.0001		1.0000	1.0000		**Aliased**

of the variation in the response variable explained by the model, and the R^2 value closer to 1 indicates a bitter fit. As shown in Table 8, the R^2 value was 0.9863 and the adjusted R^2 value was 0.9686, which is close to R^2, indicating a good fit for the model. The high R^2 and adjusted R^2 values provide a high degree of accuracy and correlation between the experimental and

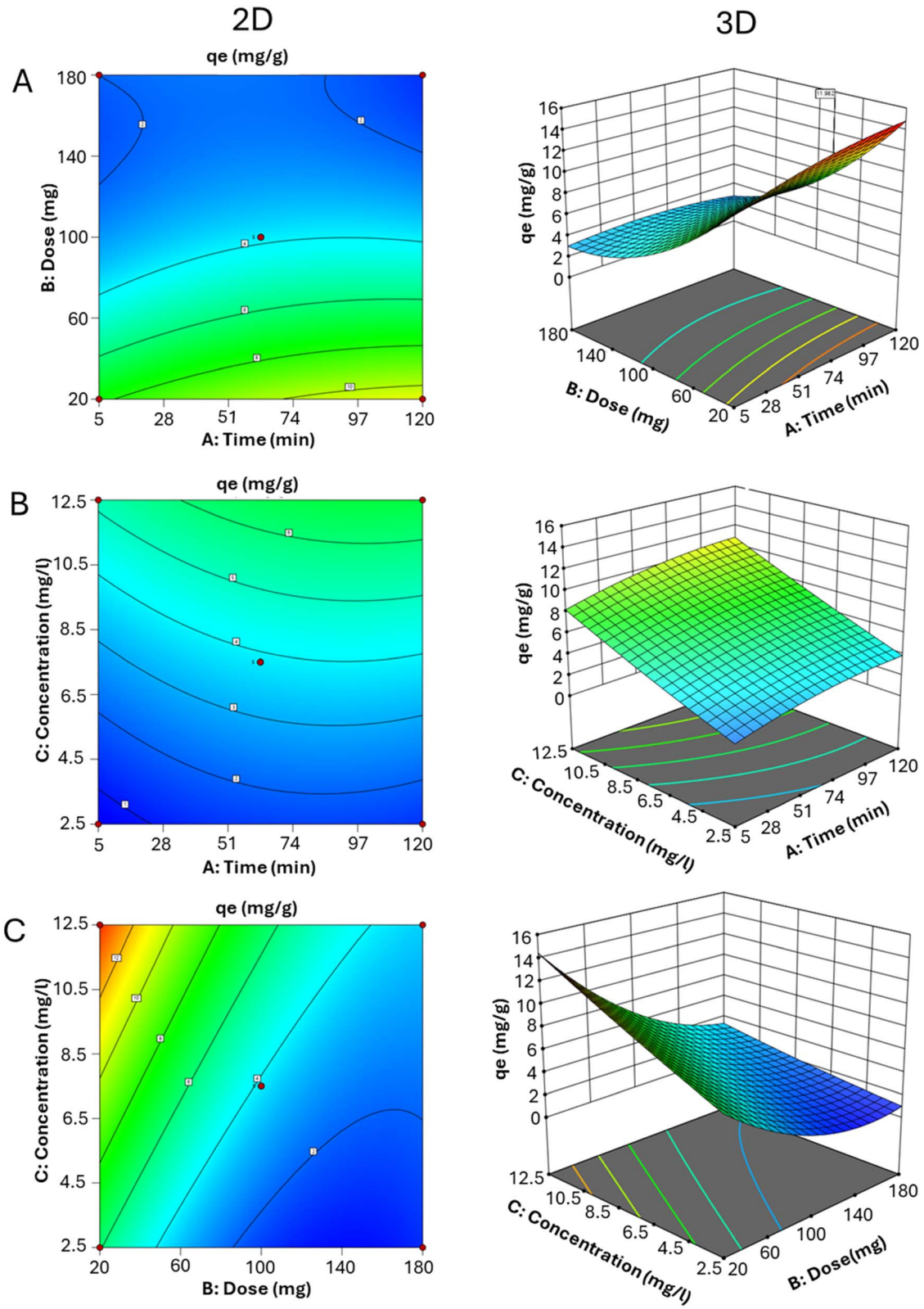

Fig. 13 Contour plots and 3D response surface representing the interaction between dose and time (A), concentration and time (B) and concentration and dose (C) for the removal of BG dye using poly(AN-*co*-AMPS).

predicted data. The predicted R^2 value of 0.7805 is in reasonable agreement with the adjusted R^2 value of 0.9686 which is less than 0.2. Adequate precision measures the signal-to-noise ratio, and a ratio greater than 4 is desirable. The model's Adeq-Prec value 27.516 indicates a sufficient signal to allow the model to be used for navigating the design space. The standard deviation is the value representing the average deviation of the observed data points from the predicted values. A lower value indicates a bitter fit of model to the data. The standard deviation of this model is 0.6309, indicating a strong agreement between prediction models and experimental data.

3.14.2. Response analysis for the adsorption capacity. The response surface plots (3D) and their corresponding contour plots (2D) are the most effective methods for understanding the effect of different parameters on the response under investigation. The response surface equation contour plot was created using the Design-Expert software to find out how various interactions affected BG's ability to adsorb onto poly(AN-*co*-AMPSP). The interaction between the adsorbent dose, contact time, and concentration of BG altering the yield of adsorption capacity was depicted using the 2-D and 3-D response surface plots. The simultaneous effect of adsorbent dose, contact time and concentration on the adsorption capacity of BG is shown in Fig. 13. As shown in Fig. 13A, first, by increasing the contact time, the BG's adsorption capacity increases, but when adsorbent dose is too high, the adsorption capacity decreases. Second, the adsorption capacity increased as the initial concentration of BG increased, and it also increased as the contact time increased, as represented in Fig. 13B. Finally, the adsorption capacity decreased as the adsorbent dose increased but it increased by increasing the initial concentration, as shown in Fig. 13C.

3.14.3. Examining the adequacy of the Box–Behnken model. The existence of data points surrounding the straight

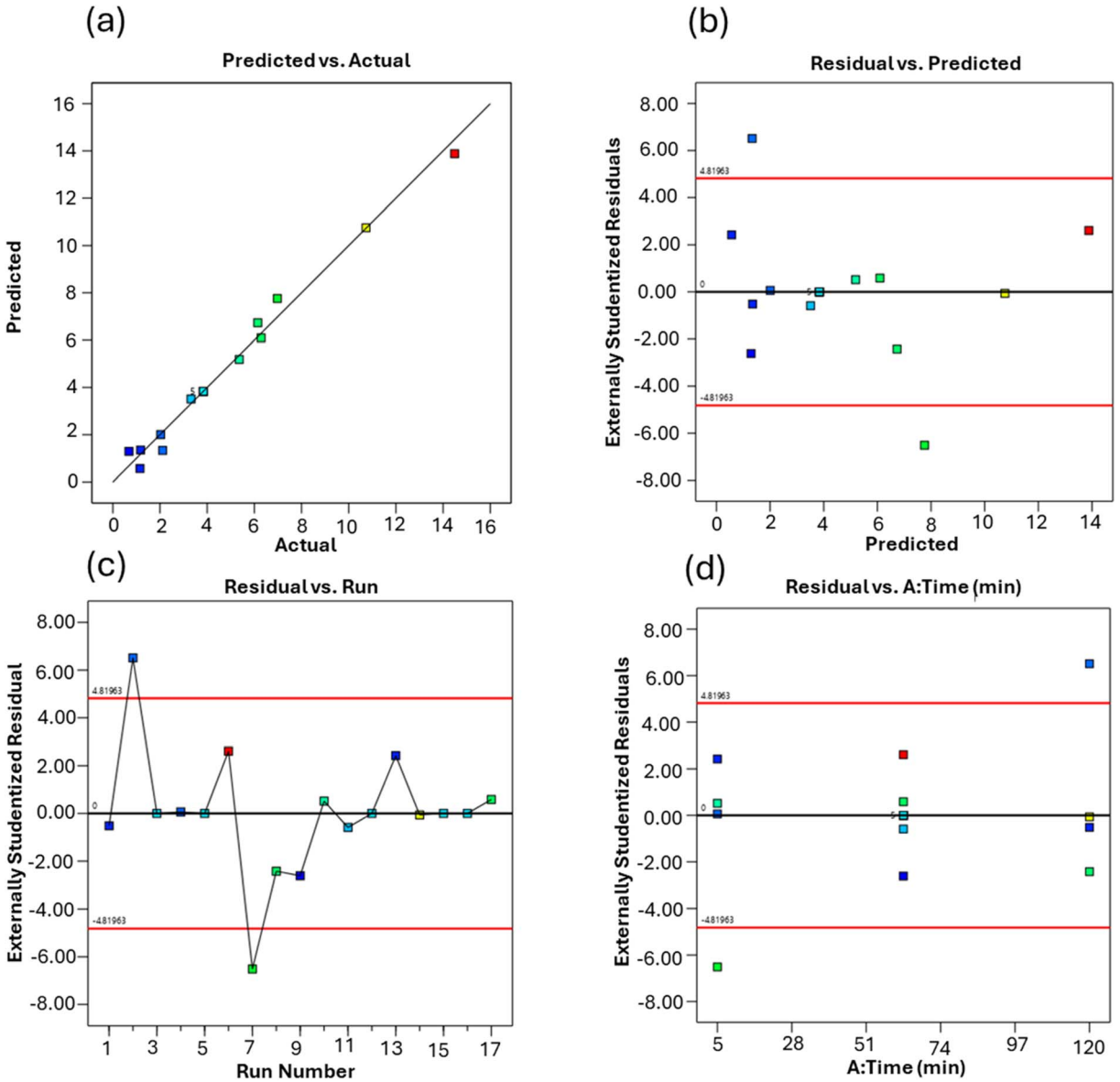

Fig. 14 (a–d) Experimental adsorption capacity *vs.* the predicted adsorption capacity.

line in Fig. 14a indicates that the actual and predicted values are close to one another, demonstrating a high level of model reliability in predicting the yield of adsorption capacity. The relation between externally studentized residuals and predicted values is shown in Fig. 14b. Standardized residuals represent the differences between the observed and predicted values, divided by the standard error. They serve as a vital diagnostic tool in regression analysis. This connection can be used to assess the overall model fit, spot potential outliers and gain an understanding of the residuals' overall trend. Fig. 14c and d, illustrates the relation between the externally studentized residuals and the run number, making it easy to show how the residuals change over the course of the experimental runs. When analyzing the experimental data, this relationship makes it possible to identify any consistent trends or anomalies that might be connected to the order of the experiment runs. Plotting the externally studentized residuals against the run numbers will reveal any residual trends that are correlated with specific run numbers. These kinds of patterns may indicate systematic errors in the procedures used to conduct the experiment, gather the data, or make measurements between runs. It is crucial to recognize these patterns to ensure the precision and consistency of the experimental results.

3.15. Comparison with other reported adsorbents

In order to assess the efficiency of poly(AN-*co*-AMPS) for removing the BG dye, we compared its removal efficiency with that of different adsorbents reported in the literature, and the data are shown in Table 9. Although comparing the removal efficiency directly is difficult due to the variety of experiment conditions such as the concentration of BG dye, the amount of adsorbent and the contact time, poly(AN-*co*-AMPS) is considered to be one of the most effective adsorbents, showing superior performance to the other adsorbents. One of the key advantages of poly(AN-*co*-AMPS) is its exceptional removal efficiency (99.5%) under relatively mild adsorption conditions (7.5 mg L^{-1} initial dye concentration, 0.1 g adsorbent dose, and 80 min contact time). Compared to activated carbon derived from cashew nut shells (CNSAC) (99% removal at 50 mg L^{-1} dye concentration) and *F. benghalensis* tree leaves (97.26% removal at 50 mg L^{-1} dye concentration), poly(AN-*co*-AMPS) demonstrates superior adsorption at significantly lower dye concentrations, indicating its high affinity for brilliant green (BG) dye. In contrast, inorganic and nanocomposite adsorbents such as ZnO/PPy nanocomposites (90.2%) and polyaniline/silver nanocomposites (90%) also exhibit high removal efficiencies but require higher synthesis costs due to the involvement of metal nanoparticles and complex preparation steps. Additionally, the hydroxyapatite/chitosan composite showed only 80% removal efficiency despite its biodegradable nature, suggesting a potential limitation in adsorption capacity. A key distinction of poly(AN-*co*-AMPS) lies in its cost-effectiveness and reusability. Unlike some adsorbents that require higher dosages (*e.g.*, kaolin at 1 g or hydroxyapatite/chitosan at 0.9 g), the synthesized copolymer achieves high removal at just 0.1 g, making it a more efficient option. Furthermore, its stability over six

Table 9 Comparison of the removal efficiency of poly(AN-*co*-AMPS) with different adsorbents for the removal of BG dye

No.	Adsorbent	Raw material	Preparation method	Reaction conditions			Removal (%)	Cost-effectiveness	Ref.
				Dye conc. (mg L^{-1})	Dose (g)	Time (min)			
1	Poly(AN-*co*-AMPS)	AN & AMPS monomers	Free radical copolymerization	7.5	0.1	80	99.5	Low-cost synthesis, high reusability	Present study
2	(CNSAC)	Cashew nut shell (biowaste)	Carbonization & activation	50	0.1	90	99	Moderate cost, renewable source	14
3	Magnetic RHA	Rice husk ash (RHA) with Fe_3O_4	Impregnation & magnetic modification	5	0.5	60	79.41	Sustainable, but higher dose required	73
4	*F. benghalensis* tree leaves	Natural tree leaves	Drying & grinding	50	0.1	60	97.26	Low-cost, but limited stability	25
5	Kaolin	Natural clay	Thermal treatment	20	1	90	91	Readily available but high dose needed	53
6	ZnO/PPy nanocomposite	Zinc oxide & polypyrrole	Chemical synthesis	90	0.075	90	90.2	High cost due to ZnO	74
7	Hydroxyapatite/chitosan composite	Chitosan & hydroxyapatite	Precipitation method	5	0.9	90	80	Biodegradable but costly	8
8	Polyacrylonitrile/silver nanocomposite	Polyacrylonitrile & silver nanoparticles	*In situ* polymerization	45.45	0.03	120	90	Expensive due to Ag content	11

successive regeneration cycles (as demonstrated in the desorption studies) further emphasizes its sustainability and economic feasibility for large-scale wastewater treatment applications.

4 Conclusions

In this study, poly(AN-*co*-AMPS), a vinyl copolymer containing amide, cyano, and sulfonic groups, was synthesized and evaluated as an effective, cost-efficient, and sustainable adsorbent for the removal of hazardous BG dye from aqueous solutions. The copolymer's unique structural properties, including high surface area and porous morphology, significantly enhanced its adsorption capacity. The presence of functional groups on poly(AN-*co*-AMPS) played a crucial role in facilitating strong interactions with dye molecules, primarily through electrostatic attraction, π–π interactions and hydrogen bond formation, leading to a high removal efficiency of 99.5% under optimal conditions. Compared to previously reported adsorbents, poly(AN-*co*-AMPS) demonstrated superior performance in terms of adsorption capacity (16.28 mg g^{-1}), faster equilibrium time (80 min), and excellent reusability, maintaining high efficiency over six consecutive regeneration cycles without any significant loss of performance. The adsorption followed the Langmuir isotherm model, indicating monolayer adsorption on a uniform surface, and the pseudo-second-order kinetic model, suggesting chemisorption as the dominant mechanism. The thermodynamic analysis confirmed the endothermic and spontaneous nature of the process, reinforcing its feasibility for real-world applications. Additionally, this study employed the Box–Behnken Design (BBD) optimization to systematically evaluate the influence of key operational parameters on adsorption efficiency. The response surface methodology provided deeper insights into the interactions between variables, allowing for an optimized adsorption process. This statistical approach enhances the practical applicability of poly(AN-*co*-AMPS) in large-scale wastewater treatment. Moreover, the copolymer's regeneration capability using HCl and its stability over multiple cycles make it a more sustainable and cost-effective alternative to conventional adsorbents. Compared to other polymeric materials, poly(AN-*co*-AMPS) offers a lower cost preparation method, high adsorption efficiency, and practical reusability, making it a promising candidate for large-scale water purification applications.

Data availability

The data supporting the findings of this study are available from the corresponding author upon reasonable request.

Author contributions

Yassin A. Aggour: supervision, project administration, resources, and writing – review & editing; El-Refaie Kenawy: supervision, investigation, and writing – review & editing; Marwa Magdy: investigation, data curation, calculation, visualization, formal analysis, methodology, and writing – original draft; Elsayed Elbayoumy: supervision, conceptualization, validation, formal analysis, investigation, resources, data curation, and writing – review & editing.

Conflicts of interest

The authors declare that they have no known competing financial interests or personal relationships that could have appeared to influence the work reported in this paper.

Acknowledgements

This research did not receive any specific grant from funding agencies in the public, commercial, or not-for-profit sectors.

References

1 K. Sukla and U. Kumar, Adsorption of brilliant green dye from aqueous solution onto chemically modified areca nut husk, *S. Afr. J. Chem. Eng.*, 2021, **35**, 33–43.
2 J. Zuo, X. Nan, L. He, Z. Xu, Z. Liu, T. Wang, *et al.*, Preparation of photo-grafted magnetic nano-silver composites and their catalytic studies on organic dyes, *Colloids Surf., A*, 2024, **684**, 133149.
3 E. Elbayoumy, M. O. Elassi, G. M. Khairy, E. A. Moawed and M. M. aboelnga, Development of efficient fluorescent sensor for the detection of hazard aromatic nitro compounds via N-(1-naphthyl)ethylenediamine: Experimental and DFT studies, *J. Mol. Liq.*, 2023, **391**(0167–7322), 123270.
4 E. Elbayoumy, A. A. El-Bindary, T. Nakano and M. M. Aboelnga, Silver nanoparticles immobilized on crosslinked vinyl polymer for catalytic reduction of nitrophenol: experimental and computational studies, *Sci. Rep.*, 2025, **15**(1), 717.
5 S. Singh, H. Gupta, S. Dhiman and N. Kishore, Decontamination of cationic dye brilliant green from the aqueous media, *Appl. Water Sci.*, 2022, **12**(4), 1–10.
6 M. K. Dahri, L. B. L. Lim, M. R. R. Kooh and C. M. Chan, Adsorption of brilliant green from aqueous solution by unmodified and chemically modified Tarap (Artocarpus odoratissimus) peel, *Int. J. Environ. Sci. Technol.*, 2017, **14**(12), 2683–2694.
7 M. T. Mosisa, P. Zhang, B. Wu, L. Chen, Z. Su, P. Li, *et al.*, Synthesis and characterization of Ce-BiOBr/Bi2S3 catalyst with enhanced catalytic activity for organic dye reduction under dark, *J. Environ. Chem. Eng.*, 2024, **12**(5), 113383.
8 A. Ragab, I. Ahmed and D. Bader, The removal of Brilliant Green dye from aqueous solution using nano hydroxyapatite/chitosan composite as a sorbent, *Molecules*, 2019, **24**(5), 847.
9 B. S. Giri, S. Gun, S. Pandey, A. Trivedi, R. T. Kapoor, R. P. Singh, *et al.*, Reusability of brilliant green dye contaminated wastewater using corncob biochar and Brevibacillus parabrevis: hybrid treatment and kinetic studies, *Bioengineered*, 2020, **11**(1), 743–758.
10 M. M. Younus, M. A. Sayed, M. El Saied and A. O. A. El Naga, Catalytic reduction of toxic dyes over nickel oxide

nanoparticles supported on CMK-3 catalyst, *Sci. Rep.*, 2024, **14**(1), 1–12.
11 O. Abd Al-Qader Mahmood and B. I. Waisi, Synthesis and characterization of polyacrylonitrile based precursor beads for the removal of the dye malachite green from its aqueous solutions, *Desalin. Water Treat.*, 2021, **216**, 445–455.
12 B. Lellis, C. Z. Fávaro-Polonio, J. A. Pamphile and J. C. Polonio, Effects of textile dyes on health and the environment and bioremediation potential of living organisms, *Biotechnol. Res. Innovation*, 2019, **3**(2), 275–290.
13 B. Saha, G. Shil, A. Debnath and B. Saha, Process optimization of victoria blue dye removal using polypyrrole-encapsulated zirconium oxide: Mechanistic pathway and economic assessment, *J. Indian Chem. Soc.*, 2024, **101**(11), 101407.
14 P. Samiyammal, A. Kokila, L. A. Pragasan, R. Rajagopal, R. Sathya, S. Ragupathy, *et al.*, Adsorption of brilliant green dye onto activated carbon prepared from cashew nut shell by KOH activation: Studies on equilibrium isotherm, *Environ. Res.*, 2022, **212**(PD), 113497.
15 M. Abbas, Removal of brilliant green (BG) by activated carbon derived from medlar nucleus (ACMN) – Kinetic, isotherms and thermodynamic aspects of adsorption, *Adsorpt. Sci. Technol.*, 2020, **38**(9–10), 464–482.
16 G. Arunkumar, G. Deviga, M. Mariappan, M. Pannipara, A. G. Al-Sehemi, U. A. Soliman, *et al.*, Carbon encapsulated ZnO nanoplates for efficient removal of organic dyes from aqueous medium by adsorption: Role of organic ligand and calcination temperature, *J. Mol. Liq.*, 2024, **403**, 124852.
17 B. K. Nandi and S. Patel, Effects of operational parameters on the removal of brilliant green dye from aqueous solutions by electrocoagulation, *Arabian J. Chem.*, 2017, **10**, S2961–S2968.
18 A. B. Bassa, O. A. Zelekew, T. A. Meresa and T. A. Berhe, Croton macrostachyus leaf-mediated biosynthesis of copper oxide nanoparticles for enhanced catalytic reduction of organic dyes, *Mater. Res. Express*, 2024, **11**(8), 085001.
19 X. Yan, M. Chen, J. Wang, Z. Wang, R. Xin, D. Wu, *et al.*, Nanoarchitectonics of bamboo-based heterojunction photocatalyst for effective removal of organic pollutants, *Chem. Eng. J.*, 2024, **495**, 153431.
20 M. A. Dominguez, M. Etcheverry and G. P. Zanini, Evaluation of the adsorption kinetics of brilliant green dye onto a montmorillonite/alginate composite bead by the shrinking core model, *Adsorption*, 2019, **25**(7), 1387–1396.
21 A. C. Enache, C. Cojocaru, P. Samoila, V. Ciornea, R. Apolzan, G. Predeanu, *et al.*, Adsorption of Brilliant Green Dye onto a Mercerized Biosorbent: Kinetic, Thermodynamic, and Molecular Docking Studies, *Molecules*, 2023, **28**(10), 4129.
22 D. Robati, B. Mirza, M. Rajabi, O. Moradi, I. Tyagi, S. Agarwal, *et al.*, Removal of hazardous dyes-BR 12 and methyl orange using graphene oxide as an adsorbent from aqueous phase, *Chem. Eng. J.*, 2016, **284**, 687–697.
23 S. Das, S. R. Paul and A. Debnath, Enhanced performance of Lagerstroemia speciosa seed biochar and polypyrrole composite for the sequestration of emerging contaminant from wastewater sample: Case study of ofloxacin drug, *J. Water Process Eng.*, 2024, **64**, 105699.
24 A. Liliana, C. Coronado-herrera, J. C. Rhenals-navarro and G. Leandro, Removal of Brilliant Green Cationic Dye Using Bioadsorbent Material from Oyster Shells, *Sustainability*, 2023, **15**(23), 16443.
25 S. Gul, A. Gul, H. Gul, R. Khattak, M. Ismail, S. U. Khan, *et al.*, Removal of Brilliant Green Dye from Water Using Ficus benghalensis Tree Leaves as an Efficient Biosorbent, *Materials*, 2023, **16**(2), 1–15.
26 N. Akter, A. Hossain, M. J. Hassan, M. K. Amin, M. Elias, M. M. Rahman, *et al.*, Amine modified tannin gel for adsorptive removal of Brilliant Green dye, *J. Environ. Chem. Eng.*, 2016, **4**(1), 1231–1241.
27 M. Luna Quinto, S. Khan, J. Vega-Chacón, B. Mortari, A. Wong, M. D. P. Taboada Sotomayor, *et al.*, Development and Characterization of a Molecularly Imprinted Polymer for the Selective Removal of Brilliant Green Textile Dye from River and Textile Industry Effluents, *Polymers*, 2023, **15**(18), 3709.
28 D. Tao, C. Tian, Y. Zhou, L. Pei and F. Zhang, Effective removal of brilliant green with magnetic barium phosphate composites: factor analysis and mechanism study, *Environ. Sci. Pollut. Res.*, 2023, **30**(17), 50364–50375.
29 M. M. Altayan, N. Tzoupanos and M. Barjenbruch, Polymer based on beta-cyclodextrin for the removal of bisphenol A, methylene blue and lead(II): Preparation, characterization, and investigation of adsorption capacity, *J. Mol. Liq.*, 2023, **390**, 122822.
30 S. Pandey, N. Son and M. Kang, Synergistic sorption performance of karaya gum crosslink poly(acrylamide-co-acrylonitrile) @ metal nanoparticle for organic pollutants, *Int. J. Biol. Macromol.*, 2022, **210**, 300–314.
31 M. R. El-Aassar, O. M. Ibrahim, B. M. Omar, H. T. A. El-Hamid, I. H. Alsohaim, H. M. A. Hassan, *et al.*, Hybrid Beads of Poly(Acrylonitrile-co-Styrene/Pyrrole)@Poly Vinyl Pyrrolidone for Removing Carcinogenic Methylene Blue Dye Water Pollutant, *J. Polym. Environ.*, 2023, **31**(7), 2912–2929.
32 M. Ajmal, S. Demirci, M. Siddiq, N. Aktas and N. Sahiner, Amidoximated poly(acrylonitrile) particles for environmental applications: Removal of heavy metal ions, dyes, and herbicides from water with different sources, *J. Appl. Polym. Sci.*, 2016, **133**(7), 1–11.
33 H. Zhang, L. Quan, A. Gao, Y. Tong, F. Shi and L. Xu, Thermal analysis and crystal structure of poly(acrylonitrile-co-itaconic acid) copolymers synthesized in water, *Polymers*, 2020, **12**(1), 221.
34 A. M. Atta, A. K. Gafer, H. A. Al-Lohedan, M. M. S. Abdullah and A. O. Ezzat, Preparation of magnetite and silver poly(2-acrylamido-2-methyl propane sulfonic acid-co-acrylamide) nanocomposites for adsorption and catalytic degradation of methylene blue water pollutant, *Polym. Int.*, 2019, **68**(6), 1164–1177.
35 A. K. Kodoth and V. Badalamoole, Pectin Based Graft Copolymer–ZnO Hybrid Nanocomposite for the Adsorptive

Removal of Crystal Violet, *J. Polym. Environ.*, 2019, **27**(9), 2040–2053.

36 Y. A. Aggour, E. R. Kenawy, M. Magdy and E. Elbayoumy, Establishing a productive heterogeneous catalyst based on silver nanoparticles supported on a crosslinked vinyl polymer for the reduction of nitrophenol, *RSC Adv.*, 2024, **14**(41), 30127–30139.

37 E. Elbayoumy, Y. Wang, M. A. R. Jamil, C. Trombini, M. Bando, Z. Song, *et al.*, Pd nanoparticles-loaded vinyl polymer gels: Preparation, structure and catalysis, *Catalysts*, 2021, **11**(1), 137.

38 C. J. Lv, H. Li, A. Yasin, B. Hao, X. Yue and P. C. Ma, Preparation of superhydrophilic poly(acrylonitrile/acrylic acid) electrospun membrane and its application in oil/water separation, *Polymer*, 2022, **258**, 125292.

39 Z. He, H. Liu, G. Yang, C. Jiang, M. Ji, J. Yu, *et al.*, Cyclization mechanism and kinetics of poly(acrylonitrile-co-2-acrylamido-2-methylpropane sulfonic acid) copolymer investigated by FTIR spectroscopy, *Polym. Test.*, 2021, **93**, 106969.

40 A. M. Atta, M. Akel, R. A. Elghazawy and M. Alaa, Characterization of modified styrene-co-2-acrylamido-2-methylpropane sulfonic acid magnetite nanoparticles, *Polym. Sci., Ser. A*, 2013, **55**(5), 327–335.

41 S. Saravanan, D. K. Sameera, A. Moorthi and N. Selvamurugan, Chitosan scaffolds containing chicken feather keratin nanoparticles for bone tissue engineering, *Int. J. Biol. Macromol.*, 2013, **62**, 481–486.

42 A. M. Atta, S. A. Sayed, A. B. Farag, H. S. Ismail, Z. M. Mohamed and A. M. Eraky, Application of crosslinked acrylamidoxime/2-acrylamido-2-methylpropane sulfonic acid copolymer in wastewater treatment, *J. Dispersion Sci. Technol.*, 2011, **32**(9), 1285–1295.

43 A. Haleem, S. B. Syaal, M. Ajmal, J. Ambreen, S. Rauf, N. Ali, *et al.*, Silver and palladium nanoparticle embedded poly(n-isopropylacrylamide-co-2-acrylamido-2-methylpropane sulfonic acid) hybrid microgel catalyst with pH and temperature dependent catalytic activity, *Korean J. Chem. Eng.*, 2020, **37**(4), 614–622.

44 E. Elbayoumy, N. A. El-Ghamaz, F. S. Mohamed, M. A. Diab and T. Nakano, Dielectric permittivity, AC electrical conductivity and conduction mechanism of high crosslinked-vinyl polymers and their $Pd(OAc)_2$ composites, *Polymers*, 2021, **13**(17), 3005.

45 M. A. Diab, N. A. El-Ghamaz, F. S. Mohamed and E. M. El-Bayoumy, Conducting polymers VIII: Optical and electrical conductivity of poly(bis-m-phenylenediaminosulphoxide), *Polym. Test.*, 2017, **63**, 440–447.

46 E. Elbayoumy, M. Elhendawy, M. M. Gaafar, E. A. Moawed and M. M. Aboelnga, Novel fluorescent sensor based on triazole-pyridine derivative for selective detection of mercury (II) ions in different real water samples: Experimental and DFT calculations, *J. Mol. Liq.*, 2024, **401**, 124589.

47 L. Zhou, Y. Wang, Q. Huang and J. Cai, Thermogravimetric characteristics and kinetic of plastic and biomass blends co-pyrolysis, *Fuel Process. Technol.*, 2006, **87**(11), 963–969.

48 N. A. El-ghamaz, T. S. Ahmed and D. A. Salama, Optical , dielectrical properties and conduction mechanism of copolymer (N , N ′ -bissulphinyl- m -benzenediamine- p -phenylenediamine), *Eur. Polym. J.*, 2017, **93**, 8–20.

49 H. S. Mahmood and M. K. Jawad, Antibacterial activity of chitosan/PAN blend prepared at different ratios, *AIP Conf. Proc.*, 2019, **2190**, 020078.

50 A. M. Atta, G. A. El-Mahdy, H. A. Al-Lohedan and A. O. Ezzat, Synthesis and Application of Hybrid Polymer Composites Based on Silver Nanoparticles as Corrosion Protection for Line Pipe Steel, *Molecules*, 2014, **19**, 6246–6262.

51 M. M. Rahman, T. Demirel, K. Ş. Tunçel and I. Karacan, The effect of the ammonium persulfate and a multi-step annealing approach during thermal stabilization of polyacrylonitrile multifilament prior to carbonization, *J. Mater. Sci.*, 2021, **56**(26), 14844–14865.

52 B. D. Zdravkov, J. J. Čermák, M. Šefara and J. Janků, Pore classification in the characterization of porous materials: A perspective, *Cent. Eur. J. Chem.*, 2007, **5**(2), 385–395.

53 B. K. Nandi, A. Goswami and M. K. Purkait, Adsorption characteristics of brilliant green dye on kaolin, *J. Hazard. Mater.*, 2009, **161**(1), 387–395.

54 M. Ali Khan, R. Govindasamy, A. Ahmad, M. R. Siddiqui, S. A. Alshareef, A. A. Hakami, *et al.*, Carbon Based Polymeric Nanocomposites for Dye Adsorption: Synthesis, Characterization, and Application, *Polymers*, 2021, **13**(3), 414.

55 N. F. Al-Harby, E. F. Albahly and N. A. Mohamed, Kinetics, Isotherm and Thermodynamic Studies for Efficient Adsorption of Congo Red Dye from Aqueous Solution onto Novel Cyanoguanidine-Modified Chitosan Adsorbent, *Polymers*, 2021, **13**(24), 4446.

56 G. Y. Abate, A. N. Alene, A. T. Habte and D. M. Getahun, Adsorptive removal of malachite green dye from aqueous solution onto activated carbon of Catha edulis stem as a low cost bio-adsorbent, *Environ. Syst. Res.*, 2020, **9**(1), 6612.

57 T. Santhi, S. Manonmani, V. S. Vasantha and Y. T. Chang, A new alternative adsorbent for the removal of cationic dyes from aqueous solution, *Arabian J. Chem.*, 2016, **9**, S466–S474.

58 M. T. Yagub, T. K. Sen, S. Afroze and H. M. Ang, Dye and its removal from aqueous solution by adsorption: A review, *Adv. Colloid Interface Sci.*, 2014, **209**, 172–184.

59 J. Hou, Y. Zhou, J. Shan, C. Gu, T. Zhang and B. Wu, Quinoline and cholesterol based organogelator for selective adsorption of cationic dyes, *Colloids Surf., A*, 2024, **700**, 134851.

60 T. M. Budnyak, M. Błachnio, A. Slabon, A. Jaworski, V. A. Tertykh, A. Deryło-Marczewska, *et al.*, Chitosan Deposited onto Fumed Silica Surface as Sustainable Hybrid Biosorbent for Acid Orange 8 Dye Capture: Effect of Temperature in Adsorption Equilibrium and Kinetics, *J. Phys. Chem. C*, 2020, **124**(28), 15312–15323.

61 N. Akter, A. Hossain, M. J. Hassan, M. K. Amin, M. Elias, M. M. Rahman, *et al.*, Journal of Environmental Chemical Engineering Amine modi fi ed tannin gel for adsorptive removal of Brilliant Green dye, *Biochem. Pharmacol.*, 2016, **4**(1), 1231–1241.

62 C. Wei, Z. Xu, F. Han, W. Xu, J. Gu, M. Ou, *et al.*, Preparation and characterization of poly(acrylic acid-co-acrylamide)/montmorillonite composite and its application for methylene blue adsorption, *Colloid Polym. Sci.*, 2018, **296**(4), 653–667.

63 Y. Hu, K. Li, Y. Li, H. Liu, M. Guo, X. Ye, *et al.*, Dyes Adsorption onto Fe_3O_4-Bis(trimethoxysilylpropyl)amine Composite Particles: Effects of pH and Ionic Strength on Electrostatic Interactions, *ChemistrySelect*, 2019, **4**(2), 617–622.

64 R. Sivaranjanee, P. S. Kumar and S. Mahalaxmi, A review on agro-based materials on the separation of environmental pollutants from water system, *Chem. Eng. Res. Des.*, 2022, **181**, 423–457.

65 M. G. El-Desouky, A. A. A. Alayyafi, G. A. A. M. Al-Hazmi and A. A. El-Bindary, Effect of metal organic framework alginate aerogel composite sponge on adsorption of tartrazine from aqueous solutions: Adsorption models, thermodynamics and optimization via Box-Behnken design, *J. Mol. Liq.*, 2024, **399**, 124392.

66 R. G. El-Sharkawy, Anchoring of green synthesized silver nanoparticles onto various surfaces for enhanced heterogeneous removal of brilliant green dye from aqueous solutions with error analysis study, *Colloids Surf., A*, 2019, **583**, 123871.

67 P. Ehiomogue, I. I. Ahuchaogu and I. E. Ahaneku, Review of adsorption isotherms models, *Acta Tech. Corviniensis*, 2022, **14**(4), 87–96.

68 T. A. Saleh, Chapter 4 – Isotherm models of adsorption processes on adsorbents and nanoadsorbents, in *Surface Science of Adsorbents and Nanoadsorbents*, ed. Saleh T. A., Elsevier, 2022, pp. 99–126.

69 M. Musah, Y. Azeh, J. Mathew, M. Umar, Z. Abdulhamid and A. Muhammad, Adsorption Kinetics and Isotherm Models: A Review, *Caliphate J. Sci. Technol.*, 2022, **4**(1), 20–26.

70 A. I. Adeogun, M. A. Idowu, A. E. Ofudje, S. O. Kareem and S. A. Ahmed, Comparative biosorption of Mn(II) and Pb(II) ions on raw and oxalic acid modified maize husk: Kinetic, thermodynamic and isothermal studies, *Appl. Water Sci.*, 2013, **3**(1), 167–179.

71 S. Rudra Paul, N. H. Singh and A. Debnath, Quick and enhanced separation of Eosin Yellow dye from aqueous solution by FeCl3 interaction: thermodynamic study and treatment cost analysis, *Int. J. Environ. Anal. Chem.*, 2022, **104**(12), 2874–2894.

72 P. S. Rudra, S. Das, A. Debnath and T. Kumar Misra, Boosted adsorptive removal of eosin yellow dye from aqueous solution with C–ZnO nanoparticles: optimization of process parameters, *J. Dispersion Sci. Technol.*, 2024, **30**, 1–17.

73 I. Dahlan, H. M. Zwain, M. A. O. Seman, N. H. Baharuddin and M. R. Othman, Adsorption of brilliant green dye in aqueous medium using magnetic adsorbents prepared from rice husk ash, *AIP Conf. Proc.*, 2019, **2124**, 020017.

74 M. Zhang, L. Chang, Y. Zhao and Z. Yu, Fabrication of Zinc Oxide/Polypyrrole Nanocomposites for Brilliant Green Removal from Aqueous Phase, *Arabian J. Sci. Eng.*, 2019, **44**(1), 111–121.